remote sensing

MDPI

Article

Structure- and Semantics-Aware Mesh Simplification for Generating Lightweight 3D Building Models

Dong Chen [1,2], Chenwei Zhu [1,2], Shenglan Du [3], Yuliang Wang [4,*], Zhen Cao [5], Mingming Sui [2], Yiyang Kong [2], Shengjie Feng [2], Jiju Peethambaran [6] and Liqiang Zhang [7]

1 Key Laboratory of Urban Land Resources Monitoring and Simulation, Ministry of Natural Resources, Shenzhen 518034, China; chendong@njfu.edu.cn (D.C.); chenweizhu@njfu.edu.cn (C.Z.)
2 College of Civil Engineering, Nanjing Forestry University, Nanjing 210037, China; mingmingsui@njfu.edu.cn (M.S.); yykong@njfu.edu.cn (Y.K.); senjerf@njfu.edu.cn (S.F.)
3 Faculty of Architecture and the Built Environment, Delft University of Technology, 2628 BL Delft, The Netherlands; shenglan.du@tudelft.nl
4 School of Computer and Information Engineering, Chuzhou University, Chuzhou 239000, China
5 The College of Geomatics and Geoinformation, Guilin University of Technology, Guilin 541004, China; caozhen@glut.edu.cn
6 Department of Mathematics and Computing Science, Saint Mary's University, Halifax, NS B3P 2M6, Canada; jiju.poovvancheri@smu.ca
7 Department of Geography, State Key Laboratory of Remote Sensing Science, Faculty of Geographical Science, Beijing Normal University, Beijing 100875, China; zhanglq@bnu.edu.cn
* Correspondence: ylw@chzu.edu.cn

Highlights

What are the main findings?

- We propose a dual-constraint edge-collapse simplification method, jointly enforcing structural constraints and semantic constraints to generate lightweight 3D building models while maintaining high geometric accuracy and semantic consistency.
- Experiments on Sketchfab, ArCH, STPLS3D and SUM datasets demonstrate the superiority of the proposed method in preserving key structural features of building models under high compression ratios compared to existing methods.

What are the implications of the main findings?

- We provide an effective approach for building model simplification, which is particularly useful for mitigating fine-scale structural degradation and semantic discontinuities commonly observed in conventional methods.
- The generated lightweight building models are enriched with both geometric details and semantic context, supporting CityGML-compliant 3D model storage, intelligent management, and downstream analysis in digital twin applications.

Abstract

Achieving lightweight representations of building mesh models with accurate geometry and fine structural details is a key challenge in urban 3D modelling. Most existing mesh simplification methods focus on minimizing geometric error while neglecting the specific characteristics of building models in terms of geometric structure and semantic hierarchy, thus leading to structural degradation and semantic inconsistencies. To address this issue, this paper proposes a structure–semantic dual-constrained edge-collapse decimation method for simplifying dense building mesh models reconstructed from point clouds. Our core innovation lies in the joint enforcement of geometric structural constraints and building semantic constraints to effectively preserve both geometric structural features and component-level semantic structures of the models. By incorporating these two constraints,

Academic Editor: Massimiliano Pepe

Received: 20 February 2026
Revised: 10 March 2026
Accepted: 15 March 2026
Published: 17 March 2026

we adaptively assign higher collapse penalties to key structural edges and semantic boundaries, achieving lightweight building model simplification while maintaining fine-level structural details even under high compression ratios. Our method is extensively validated on several datasets of varying scales and complexities, including single-building models from Sketchfab, the large-scale urban datasets SUM and STPLS3D, and the ArCH cultural heritage dataset. Experimental results demonstrate that our method achieves superior or comparable performance compared to the existing methods across all the test datasets, consistently achieving lower or on-par geometric errors measured by RMSE and MAE. Furthermore, our simplified results can be semantically organized and stored under the CityGML paradigm, which provides a unified data support for sharing, semantic retrieval, downstream analysis, and other applications of lightweight building models.

Keywords: urban modelling; building mesh simplification; digital twins; structural semantics; building point clouds

1. Introduction

3D building models, the core of digital representation of urban cities, have been widely applied in urban planning [1], city construction [2], navigation and autonomous driving [3], entertainment industries [4], and virtual reality [5]. With the recent development of low-altitude economy as well as the rapid advancements of fundamental surveying and mapping technologies, application demands for 3D building models are progressively shifting from traditional "storage and visualization" toward "support for intelligent analysis, simulation and computation." High-quality 3D building models not only provide fundamental geographic entity representations for smart city development, but also serve as a critical data support for spatial computation in complex scenes, urban energy analysis, transportation route planning, and urban facility maintenance [6].

Light detection and ranging (LiDAR) point clouds are one of the most important data sources for constructing digital 3D building models in urban scenes. By measuring the laser time of flight and solving for the coordinates of target points, LiDAR provides 3D point cloud data with high accuracy, long detection range, and low sensitivity to illumination variance. 3D building reconstruction from LiDAR point clouds typically involves approaches such as planar segmentation [7,8], primitive fitting and matching [9,10], energy-based optimization [11,12], and mesh-based simplified modelling [13–15]. Among these approaches, mesh models are widely used for reconstructing building façades and components, mainly due to their high geometric fidelity, rendering efficiency, and simple data structures. By leveraging 3D reconstruction techniques, such as Poisson reconstruction [16], ball-pivoting surface reconstruction [17], and Alpha Shapes [18], dense mesh models can be generated with continuous geometric and topological information. Despite that dense mesh models preserve rich geometric details, they often incur high costs in data storage, transfer, visualization, and rendering [19]. To reduce such computational and memory costs, a number of studies construct lightweight 3D building models by adopting geometric abstraction strategies such as regularized block representations [20–22] or primitive matching [23–25] to achieve model simplification. However, these methods, which rely on increasing the level of abstraction, inevitably reduce geometric accuracy and lead to substantial loss of structural details of buildings. In contrast to parametric reconstruction based on primitive fitting and model abstraction via surface fitting or energy-based optimization, mesh model simplification methods directly based on point clouds better retain the true geometry of

buildings with enhanced geometric representational capability. Therefore, they are by nature more suitable for high-fidelity building reconstruction in complex urban scenes.

Mesh simplification methods aim to reduce the number of vertices and faces in a polygonal mesh model, while preserving its geometric fidelity. In the fields of computer graphics and 3D computer vision, various simplification strategies have been proposed based on different principles, including vertex removal [26,27], vertex clustering [28,29], and edge-collapse algorithms [13,30,31]. Lindstrom and Turk [31] introduced a fast and efficient edge-collapse simplification method. Their core idea is to incorporate constraints to preserve the model volume and boundary area during edge collapse and vertex position optimization, thereby maintaining the global geometric shape of the model. Garland and Heckbert [13] proposed performing edge collapse based on the quadric error metrics (QEM), associating each vertex with a quadric error matrix derived from its adjacent faces and using this error as the cost function to guide the edge-collapse process. Given its good trade-off among efficiency, robustness, and generality, the QEM method and its variants have become the mainstream framework for 3D mesh simplification tasks in general scenes. Nevertheless, as the QEM algorithm applies uniform simplification to all parts of a mesh model, it does not take into account the importance of individual architectural components. Thus, it often fails to preserve geometric details and structural characteristics of building components, which weakens the appearance regularity of man-made buildings [32]. When directly applied to building model simplification, it can lead to oversimplification, geometric distortions, and structural degradation, resulting in issues such as roof fragmentation, blurred ridgelines, and facade collapse. These issues are particularly pronounced on complex architectural buildings, e.g., cultural heritage architecture. Consequently, ideal building model simplification must not only maintain geometric accuracy but also preserve architectural geometric structure, which suggests a multi-objective optimization problem by jointly considering geometric fidelity, model compactness, and structural integrity. In response to this problem, how to achieve mesh simplification that ensures high geometric accuracy, architectural structural fidelity, and lightweight building representations has become a central research focus in the field of 3D reconstruction [33].

In subsequent studies, researchers have introduced additional architectural geometric constraints into the edge-collapse cost function, based on different definitions and interpretations of building geometric structure, with the goal of suppressing structural degradation of critical architectural elements during simplification [14,15,34–37]. For example, volume-preservation constraints are employed to prevent global shrinkage of buildings [34]; curvature-related constraints are used to increase the collapse cost in high-curvature regions to retain highly curved features [35]; normal-consistency constraints are incorporated to avoid large-angle flips of faces after edge collapse [36]. Li and Nan [14] interpreted architectural geometric structures as regular planar components, proposing to apply bilateral filtering prior to mesh simplification to enhance planar geometric features. Then, architectural planar structures such as roofs and facades can be identified through region growing and merging. Their obtained building models exhibit planar geometric structures with improved regularity. Salinas et al. [37] introduced a structure-aware mechanism into the mesh simplification. By segmenting meshes into multiple regions through region growing, vertices that preserve intra-region consistency and structural adjacency relationships, as well as corner vertices, are recognized as key architectural structural vertices and are imposed with corresponding geometric constraints during edge collapse, which effectively preserves architectural structural integrity at high compression ratios. However, the performance of this method largely depends on the quality of structural region partitioning, which is sensitive to initialization and parameter settings. Li et al. [15] employed the gradient structure tensor [38] as a metric to identify key architectural struc-

tural vertices, incorporating it as a geometric constraint into the edge-collapse decision process. Furthermore, different primitive types, such as linear primitives, nonlinear primitives, and structural feature edges, are assigned different weights. The collapse costs of roof skeleton edges, building ridgelines, and facade contour edges, which are often regarded as key architectural geometric structures, are increased, preventing their early collapse in the simplification process. In other words, the edge-collapse order is no longer solely determined by a uniform local geometric error metric, but is instead guided by architectural geometric structure constraints. The overall principle behind this design is to identify key architectural structures and assign them higher weights, so as to preserve critical building regions at different levels.

Geometric-structure constraints can partially maintain the stability of local geometries in building models. However, they fail to adequately account for the semantic importance of different architectural components. The semantic structure of building components does not necessarily correspond to regions of geometric discontinuity. Rather, its core lies in describing the structural delineation among different components. Under high compression ratios, lightweight models relying purely on geometric constraints tend to produce cross-component folding and erroneous merging of semantically distinct parts, which compromises both the structural interpretability and component integrity of building models. Therefore, it is necessary to further exploit building semantics to mitigate the loss of geometric fidelity induced by purely geometry-driven simplification methods.

Currently, the two most widely used semantic modelling standards for buildings, CityGML [39] and IFC [40], have developed comprehensive description schemes that integrate geometric and semantic information for 3D building models, allowing them to encode hierarchical structures, functional semantics, material properties, and other auxiliary attributes. In the meantime, several publicly available building point cloud datasets, such as the cultural heritage building dataset ArCH [41], the building facade dataset ZAHA [42], and the large-scale urban building dataset DublinCity [43], also provide rich semantic annotations. As pointed out by Chen et al. [6], the criterion for evaluating building model quality is shifting from a "data-driven" paradigm, which focuses on geometric accuracy and topological correctness, toward an "application-driven" perspective that jointly considers multimodal expressiveness and application-oriented suitability. Traditional simplification strategies relying purely on geometric-structure constraints can successfully reduce the geometric complexity of building models, but cannot prevent the degradation of semantically critical building components. By introducing semantic–structure constraints into model simplification, key structural regions of buildings can be explicitly identified, and essential components can be prioritized and preserved through semantic weighting [19]. Consequently, this approach increases the effective information density of the simplified model while reducing redundancy [44]. Moreover, the enriched semantic information retained in the simplified building models can greatly improve model interpretability and extensibility for downstream applications.

At present, there are limited research studies on building model simplification guided by semantic–structure constraints. Fan et al. [45] explored how to generate highly abstracted building models from CityGML-based representations through semantic aggregation and geometric generalization. This approach reduces volumetric walls to single planar surfaces and eliminates detailed linear features on facades. In their subsequent work, Fan et al. [46] introduced a method that converts irregular LoD2 building models with geometric details into regularized and simplified models by directional clustering and boundary normalization, while maintaining the model's semantic structural integrity. Zhu et al. [47] further reorganized the semantic information of building models defined under the IFC standard and converted them into simplified CityGML representations with

multiple levels of granularity (LoD1–LoD4), effectively reducing the model complexity under the constraint of semantic consistency. Under the semantic modelling framework of IFC, Wu et al. [48] introduced a semantic similarity metric for CityGML building models, where surface meshes with higher semantic similarity are preferentially merged to achieve lightweight representations of buildings across different levels of detail (LoDs). For large-scale urban mesh scenes, Xia et al. [49] extracted a set of geometric descriptors, including curvature, flatness, and anisotropy, to partition mesh vertices into four semantic classes (i.e., ground, roof, facade, and clutter). The priority of edge collapses was adaptively adjusted based on semantic differences to achieve semantics-aware building simplification at the city scale.

In summary, existing research on building model simplification under semantic–structure constraints can be categorized into two main directions: The first focuses on semantic generalization and LoD degradation under CityGML or IFC standards, where building models are simplified through semantic aggregation and component regularization. The second direction investigates semantics-aware simplification targeting urban scene elements. In this category, semantic constraints are designed at the generic urban scene level rather than the individual building-instance level. Moreover, the semantic description of building structures is often confined to roofs and facades. The former direction of approaches relies heavily on the predefined semantic hierarchies and data schemas of CityGML and IFC. The latter, although incorporating building structures as constraints in the simplification process, is limited to coarse-grained urban-scene level semantics and fails to explicitly model structural boundaries among different building components. To date, building model simplification under explicit semantic–structure constraints at the building component level has not been adequately explored. Without semantic constraints at the building-component level, model simplification targeting high reduction ratios is prone to cross-component folding, which can significantly impair structural boundary lines of key components such as doors, windows, and facades. This issue often appears in building models with complex geometries and rich structural details, such as cultural heritage and historical buildings. For these buildings, edge collapses crossing semantic boundaries can lead to semantic inconsistencies of the building components, thus severely degrading the model's interpretability and application value.

In this paper, we explicitly address the issues of geometric degradation and semantic inconsistency in the task of building model simplification under high compression ratios. We propose a dual-constrained building model simplification method by jointly considering geometric structures and semantic structures at the building component level. This method integrates geometric and component semantic constraints into the traditional QEM-based edge collapse framework. By adaptively regulating the edge-collapse cost function and collapse sequence, it achieves effective building model simplification under high compression ratios, while maintaining its geometric accuracy with enhanced structural interpretability.

Unlike existing methods that purely rely on geometric constraints or structural priors, the proposed approach does not require prior knowledge of building geometry. Instead, it adaptively adjusts the folding priority by jointly combining geometric features and semantic guidance of building components, which can be robustly applied in various building scenes with different scales and structural complexities. Based on this design, our generated lightweight building mesh models remain consistent between geometric structures and semantic components, further supporting standardized transformation and data storage under the CityGML standard to achieve an integrated 3D building representation of geometric, topological, and semantic information.

The main contributions of this paper are summarized as follows:

- We propose a dual-constraint mesh edge-collapse simplification method that jointly considers geometric structure and building semantic components. Focusing on high-density building mesh models reconstructed from point clouds and enriched with building component semantics, both geometric structural constraints and semantic structural constraints are incorporated for model simplification. Edges associated with key geometric structures or critical semantic components are assigned higher collapse penalties to postpone their collapse order. In this way, we effectively preserve building structural details and critical semantic components while maintaining high compression ratios. Furthermore, the generated lightweight semantic building mesh models are standardized and stored under the CityGML standard, enabling an integrated representation of geometric, topological, and semantic information. This facilitates efficient retrieval of semantic building components and supports computational and analytical downstream applications.
- We propose a building model simplification method based on geometric structural constraints. We construct two metrics, geometric saliency derived from the covariance of three-ring neighbourhoods and local normal inconsistency, to identify key geometric structural points in building mesh models. Then, we incorporate geometric structural constraints to optimize the edge-collapse sequence. Without additional structural priors, the method adaptively increases the collapse cost in key structural regions to preserve critical geometric structures under high compression ratios. This effectively prevents triangle flipping and local shape degradation, and also enhances the geometric stability and structural fidelity of the resultant models.
- We introduce semantic structural lines of building components as constraints in edge-collapse simplification, which are extracted by projecting the semantic point cloud onto the mesh to identify semantic conflict edges. Laplacian deformation is applied to align the original mesh with the regularized semantic structural lines. Then, semantic constraints are incorporated into the edge-collapse cost function to postpone the collapse of edges of semantic component boundaries during simplification, thus preventing semantic inconsistencies resulting from edge collapses across component boundaries at roofs, facades, and building component junctions. In this way, we achieve a unified preservation of geometric structure and semantic structure in the simplified building models.

The proposed method was evaluated on multiple finely detailed single-building models randomly selected from the Sketchfab open data platform [50], large-scale building datasets (SUM [51] and STPLS3D [52]), and a dataset with building component semantic annotations (ArCH [41]). Our algorithm was compared with the three simplification approaches proposed by Garland and Heckbert (GH) [13], Lindstrom and Turk (LT) [31], and Campen et al. (SLA) [37], respectively. We compared our results at different compression ratios from the perspectives of geometric accuracy and model structural preservation. For quantitative evaluation, we employed Root Mean Square Error (RMSE) and Mean Absolute Error (MAE) to calculate the geometric deviation of the simplified models with respect to the reference models.

2. Methodology

We introduce an improved edge-collapse simplification method jointly optimized by geometric and semantic constraints for lightweight simplification of dense building mesh models. The input is a dense building mesh model with component-level semantic information (see Figure 1b), where building component semantics are provided by manually annotated semantic point clouds and transferred to the building mesh via point-to-mesh

projection. Note that our method does not depend on a specific semantic acquisition strategy. For building mesh models that do not directly contain semantic information, building component semantics can alternatively be obtained by deep learning-based semantic segmentation methods or other approaches. These semantics can then also serve as input for constructing building semantic constraints, providing users with flexibility in semantic data acquisition when using our method.

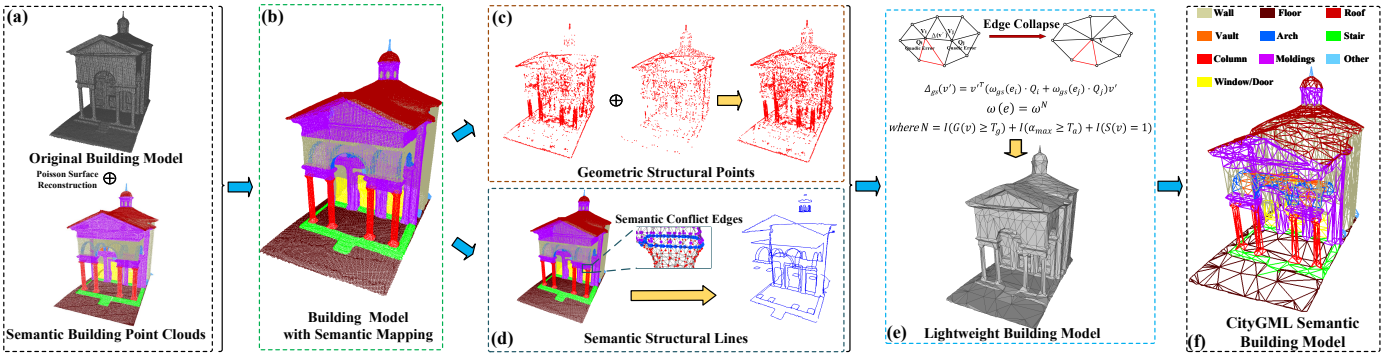

Figure 1. Pipeline of Structure- and Semantics-Aware Mesh Decimation for Efficient 3D Building Models. Subfigure (**a**) shows the building semantic point cloud and the original mesh reconstructed via Poisson surface reconstruction. Subfigure (**b**) presents the input building mesh after semantic projection. Subfigure (**c**) illustrates the identification of geometric structural points based on vertex geometric saliency and local normal inconsistency. Subfigure (**d**) shows the extraction and regularization of component semantic structural lines from semantic conflict edges. Subfigure (**e**) demonstrates the edge-collapse simplification process under joint geometric structural and component semantic constraints. Subfigure (**f**) presents the final lightweight semantic building model under the CityGML paradigm.

Our simplification method consists of two constraint terms: (1) a building geometric structural point constraint based on vertex geometric saliency and local normal inconsistency, and (2) a semantic component structural edge constraint derived from the extracted semantic conflict edges. From the geometric perspective, critical geometric structural points are identified from two aspects: local spatial shape variation and normal inconsistency (see Figure 1c). First, based on the distribution of covariance eigenvalues within three-ring neighbourhoods, we calculate a multi-scale fused geometric saliency metric, which characterizes the anisotropy and degree of morphological variation in the local spatial distribution of vertices. Using this metric, we can effectively distinguish vertices with salient structural features from the rest of the vertices. Subsequently, we measure the local normal inconsistency by computing the maximum angular deviation between the normals of adjacent triangular faces in the one-ring neighbourhood and the centroid vertex normal, in order to assess the potential risk of normal discontinuities and triangle flipping during edge collapse. We consider both the geometric saliency and the local normal inconsistency to form the geometric structural constraint. Local vertices with high shape variation and low normal inconsistency are assigned higher collapse costs to avoid early collapse of these critical structural points. This greatly reduces triangle flipping and local geometric degradation and achieves stable preservation of the geometric structure of building models under high compression ratios. From the semantic perspective, we project a semantic point cloud annotated with building component labels onto the high-density mesh surface reconstructed by Poisson reconstruction, and, accordingly, extract building component semantic structural lines (see Figure 1d). Edges corresponding to these semantic structural lines are assigned additional weights to increase their collapse costs, postponing their priority in edge-collapse simplification.

By jointly combining geometric structural constraints and building component semantic constraints, the proposed approach utilizes complementary information to achieve mutual enhancement in the edge-collapse process. Both geometric structural features and building component semantic structures are well preserved during simplification, which improves the overall quality of the simplified models in terms of geometric accuracy and structural stability.

2.1. Geometric Structural Points

In 3D building models, vertices at structural turning locations, component boundaries, or fine-grained local regions play a significant role. Collapsing such vertices directly affects the global morphology and structural interpretability of the building model. These vertices, which serve essential structural functions in building geometric representation, are referred to as building geometric structural points in this study. Building geometric structural points includes two types. First, the vertices located on ridges, edges, and geometrically discontinuous regions formed by the intersection of different structural surfaces, which exhibit significant anisotropy and morphological variation in local neighbourhoods; Second, vertices in regions with abrupt normal variations. Collapsing such vertices can potentially lead to triangle flipping or local geometric degradation. Both types of points correspond to key structural lines or fine-scale components in building models and serve as essential elements for maintaining geometric stability and structural fidelity. Therefore, in this study, we identify geometric structural points from both perspectives of the local spatial shape variation and the normal inconsistency.

From the local shape variation perspective, we introduce the metric of geometric saliency to reflect the degree of local shape variation of a vertex in spatial domains. For an arbitrary vertex v_i, its local neighbourhood $N_r(v_i)$ is defined as the set of vertices with an adjacency depth of r centered at v_i. The geometric centroid of its r-ring neighbourhood is computed as follows:

$$\bar{p}_i^{(r)} = \frac{1}{|N_r(v_i)|} \sum_{p_j \in N_r(v_i)} p_j \tag{1}$$

where p_j is the position of its j^{th} neighbour, and $|N_r(v_i)|$ represents neighbourhood cardinality. The neighbourhood covariance matrix is computed as follows:

$$C^{(r)}(v_i) = \frac{1}{|N_r(v_i)|} \sum_{p_j \in N_r(v_i)} \left(p_j - \bar{p}_i^{(r)}\right)\left(p_j - \bar{p}_i^{(r)}\right)^T \tag{2}$$

The covariance matrix $C^{(r)}(v_i)$ characterizes the principal directions and dispersion of the local geometric distribution around a vertex. Its Eigen-decomposition yields three eigenvalues $\lambda_1 > \lambda_2 > \lambda_3$, representing variances along the principal direction, secondary direction, and surface normal direction of the local neighbourhood, respectively. To quantify the stability and saliency of the local geometric structure, we define an Eigen-based saliency metric using the following equation:

$$\kappa_i^{(r)} = \frac{\lambda_3}{\lambda_1 + \lambda_2 + \lambda_3} \tag{3}$$

On a planar region, $\lambda_3 \ll \lambda_2 < \lambda_1$, resulting in $\kappa_i^r \approx 0$, while at curves or edges, the variances along the three directions tend to be comparable, which indicates a higher κ_i^r

and an increased vertex saliency. We fuse the saliency values across three neighbourhoods through a weighted combination to achieve robustness and multi-scale stability:

$$G(v_i) = \sum_{r=1}^{3} W_r \, \kappa_i^{(r)}, \quad W_r = \frac{1}{r} \tag{4}$$

The weighting scheme ensures that the inner neighbourhoods are more sensitive to local morphological variations, and the outer neighbourhoods provide an overall stabilizing influence. The obtained $G(v_i)$ is normalized between 0 and 1:

$$G(v_i) = \frac{G(v_i) - G_{\min}}{G_{\max} - G_{\min}} \tag{5}$$

The geometric saliency metric $G(v)$ basically reflects the degree of anisotropy in the spatial distribution of a vertex's local neighbourhood. In planar regions, its value is relatively low. However, $G(v)$ increases when confronting large local shape variations, such as ridges, intersecting surfaces, or fine structural details. Vertices with high $G(v)$ are critical geometric structural points. Wrongly collapsing these vertices at an early stage can propagate errors, induce structural degradation, and ultimately affect the quality of the simplified model. Therefore, in this study, we adopt a conservative strategy to prioritize the preservation of these geometric structural points. We use $G(v) \geq T_g$ as one of the criteria for identifying geometric structural points. T_g is empirically set to 0.65. This threshold is selected to cover the majority of geometrically salient vertices without excessively including non-structural points, providing a stable candidate set for subsequent edge-collapse optimization.

Moreover, sharp features of buildings often exhibit large normal deviations in their local neighbourhoods, which tend to induce triangle flipping and local detail degradation during the edge-collapse process. To cope with this issue, we propose to further identify geometric structural points by evaluating local normal inconsistency. The metric of local normal inconsistency measures the maximum deviation between the normals of one-ring neighbouring faces and the centroid vertex normal. Incorporated as a collapse-error constraint, it significantly increases the collapse cost in corner and sharp-feature regions to preserve these sharp details, while preventing local geometric degradation due to large face rotations. Given the three vertices v_i, v_j, v_o of an arbitrary mesh, the normal of this mesh can be derived from the following equation:

$$n_i = \frac{(v_j - v_i) \times (v_o - v_j)}{\left\| (v_j - v_i) \times (v_o - v_j) \right\|} \tag{6}$$

Let k denote the number of triangular faces in the one-ring neighbourhood of vertex V_i. The vertex normal n_{v_i} is computed as the weighted average of the surrounding face normals, with weights given by the face areas S_i:

$$n_{v_i} = \frac{\sum_{i=1}^{k} S_i \, n_i}{\left\| \sum_{i=1}^{k} S_i \, n_i \right\|} \tag{7}$$

The local normal inconsistency metric α is derived accordingly:

$$\alpha_{\max} = \max_{k} \ \arccos(n_{v_i} \cdot n_k) \tag{8}$$

We use $\alpha_{max} \geq T_\alpha$ as an additional criterion for identifying geometric structural points, with T_α empirically set to 60°. This threshold effectively covers sharp features of the build-

ing model. It can also discriminate between normal variations resulting from architectural geometric changes and minor perturbations due to local noise or reconstruction errors. Thus, the criterion enables the method to impose geometric structural constraints only on critical regions that are prone to face flipping or structural degeneration.

Overall, the geometric structural points defined in this paper are jointly determined by geometric saliency and local normal inconsistency. The former metric characterizes abrupt changes in local shapes, enabling the detection of ridges and fine structural details in buildings. The latter focuses on preserving sharp features, which prevents normal discontinuities and face flipping that may arise during the simplification process. Collectively incorporating the two metrics into the geometric structural constraints allows our proposed algorithm to maintain structural integrity and geometric stability of building models, even under high compression ratios.

2.2. Building Component Semantic Structural Lines

Semantic structural components play a significant role in 3D building models. On the one hand, incorporating semantic constraints guides the simplification algorithm to preserve semantically important components of the model. On the other hand, it also enhances the model expressiveness by embedding enriched semantic information. From a broader point of view, building semantics refers to a high-level description of the structural categories, functionalities, and spatial relationships of the building elements. Unlike geometric representations, semantics emphasizes structural relationships and functional differentiation among components, which provide a data foundation for interpretable and analyzable building models. In this study, we explicitly define building semantics at three hierarchies: structure, primitive, and component. At the structural scale, the building is abstracted into macro units such as roofs, facades, and bases to characterize its global organizational pattern. At the primitive scale, geometric primitives such as wall planes, roof planes, and nonlinear free-form surfaces are defined to represent the fundamental geometric units of buildings. At the component scale, architectural attachments such as doors, windows, balconies, skylights, chimneys, and decorative elements are incorporated to describe functional and fine-grained local structures. By simultaneously considering semantic representations at all three hierarchies, our method allows the structured organization and inheritance of multiscale semantic information of building mesh models. Furthermore, the building semantic structures do not necessarily reflect local shape variations. Rather, we use them to delineate structural boundaries between different building components. When an edge in a mesh model comprises two vertices from different semantic categories of building components, this edge is structurally important for preserving the model's component integrity and interpretability. Driven by this observation, we define semantic conflict edges as the edges associated with inconsistent building-component semantics. The corresponding structural boundaries are referred to as semantic structural lines.

We first project a building semantic point cloud containing component labels onto the dense building mesh model reconstructed via Poisson surface reconstruction [16]. To achieve this, a KD-tree spatial index is constructed for the semantic point cloud. The semantic label of the nearest semantic point is then assigned to each mesh vertex using a nearest-neighbor search strategy. The output is a building mesh model annotated with semantic labels. Figure 2a visualizes the vertices of the building model after semantic mapping. If the two vertices of an edge belong to different semantic components (e.g., a wall and a door or window), the edge is identified as a semantic conflict edge, which intrinsically reflects the structural connectivity between building components. Based on semantic conflict edges, we primarily extract semantic structural lines on the mesh model, as shown in Figure 2b. However, the semantic structural lines generated directly

through semantic mapping often exhibit irregular artifacts and redundant isolated edges. To address these issues, we further regularize the semantic structural lines using pruning and median smoothing. Specifically, short connected branches with connectivity depth lower than a predefined threshold ($\tau = 5$), which are typically caused by semantic noise or local labeling errors, are first removed. For each remaining semantic structural edge, its middle point is derived by averaging its endpoints. By recovering the original topological connectivity, a new set of smooth and continuous structural lines is obtained. The semantic structural points are then projected onto the regularized structural lines to obtain the refined semantic structural lines of building components, as shown in Figure 2c. The refined semantic structural lines are geometrically more regular and better conform to the linear characteristics of architectural geometry. Meanwhile, the regularization process does not change the number of semantic structural points or their topological connectivity.

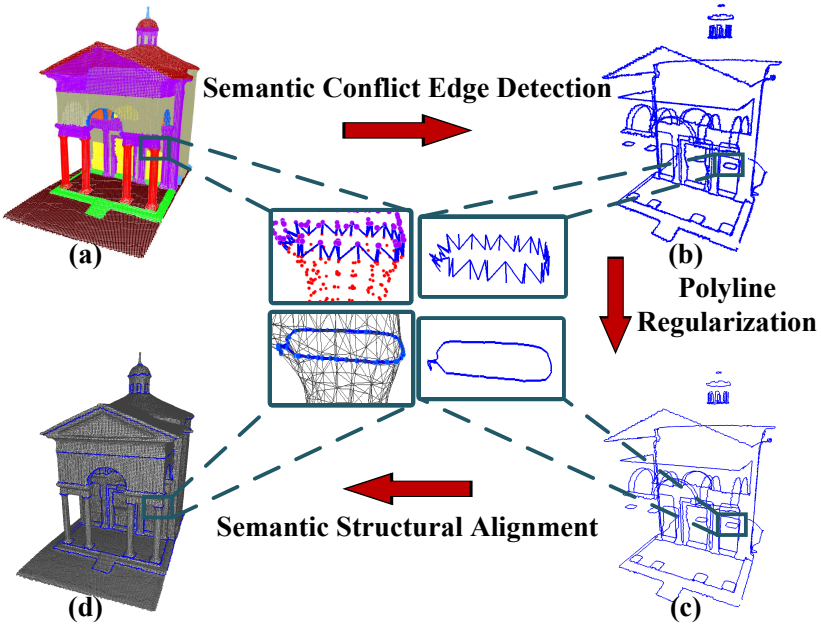

Figure 2. Extraction and regularization of building component semantic structural lines. Subfigure (**a**) presents the building semantic points after semantic projection. Subfigure (**b**) illustrates the initial component semantic structural lines derived from semantic conflict edges. Subfigure (**c**) depicts the regularized component semantic structural lines. Subfigure (**d**) demonstrates the building model aligned with the regularized semantic structural lines.

Subsequently, we adopt Laplacian deformation [53] to align the semantic structural lines on the original mesh with the regularized semantic structural lines to ensure their spatial consistency and encourage smooth local geometric transitions. Laplacian deformation is widely used in animated 3D modelling, 3D editing, and interactive geometric modelling, which aims to achieve smooth model deformation under predefined constraints while preserving the original local geometry as much as possible. Here, we introduce Laplacian deformation as an adjustment mechanism to align the geometry of the original building model with the regularized semantic structural lines. Unlike methods that directly replace or project vertex coordinates, Laplacian deformation constrains the local differential positions within the one-ring neighbourhood and formulates the adjustment as an energy minimization problem (see Figure 3). It effectively repositions the semantic structural lines while propagating the geometric deformation smoothly to the surrounding regions to avoid potential geometric discontinuities or local shape distortions. Differential positions characterize the local geometric relationships of a vertex with respect to its neighbourhood. Through Laplacian deformation, these relationships remain stable, meaning that the ad-

justment of semantic structural lines does not impair the intrinsic mesh connectivity of the building model.

Let $\{v_i\}$ denote the vertex set of the original mesh, and C the set of points on the regularized semantic structural lines. The Laplacian energy function based on differential positions is defined as follows:

$$E_L = \sum_i \| Lv_i' - \delta_i \|^2 + \lambda_c \sum_{j \in C} \left\| v_j' - c_j \right\|^2 \quad (9)$$

where v_i' is the deformed position of the i^{th} vertex in the mesh, L represents the Laplacian matrix, $L_{v_i'}$ is the local differential position of the vertex with respect to its neighbourhood after deformation, λ_c is the deformation constraint weight to align the semantic structural lines of the original mesh with the regularized lines, $\delta_i = \frac{1}{d_i} \sum_{j \in N(i)} (v_i - v_j)$ is the local differential position of vertex v_i within its one-ring neighbourhood $N(i)$ in the original mesh, d_i is the number of neighbouring vertices, v_j is the position of a building-component semantic structural point in the original mesh, v_j' is its deformed position, and c_j represents the target position of v_j on the regularized semantic structural line.

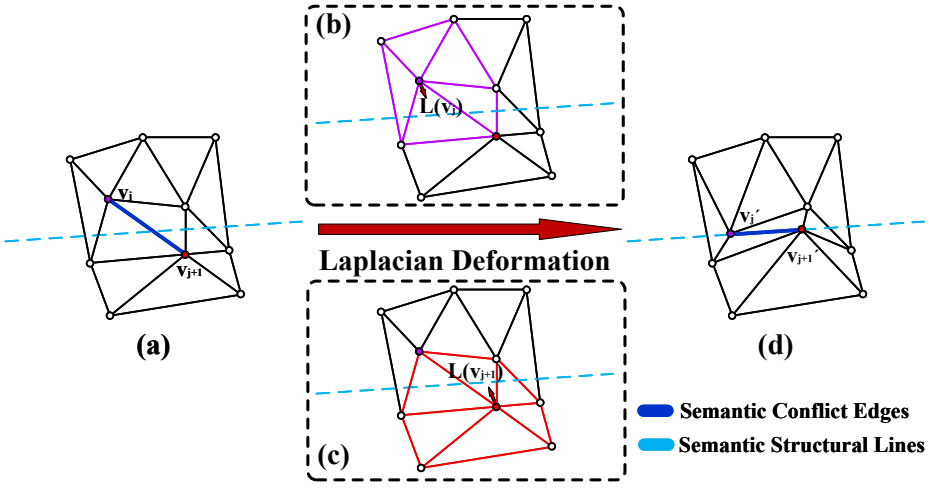

Figure 3. Alignment of building component semantic structures based on Laplacian deformation. Subfigure (**a**) presents the semantic conflict edges in the original building mesh caused by different component semantics, where purple and red points indicate vertices belonging to different semantic components. Subfigures (**b**,**c**) illustrate the local geometric adjustment of semantic structural points through Laplacian energy optimization within the one-ring neighbourhood. Subfigure (**d**) demonstrates the alignment result, where semantic structural points of the original building model are pulled onto the regularized semantic structural lines.

The first energy term preserves the local geometry, and the second term enforces the semantic structural points on the original mesh to accurately fit the target positions on the regularized semantic structural lines.

For solving the Laplacian deformation problem, we adopt the Spokes-and-Rims deformation solver [54] provided in the Surface Mesh Deformation framework of the Computational Geometry Algorithms Library (CGAL). This approach introduces a local rotation matrix R_i within each neighborhood to improve rotational invariance during the deformation. It also replaces the first differential coordinate energy term in Equation (9) with a local rigidity-preserving energy formulation to enhance the stability and structural fidelity of the resulting mesh.

For each edge $(i, j) \in E$ in the mesh, let the two end vertices before and after deformation be (v_i, v_j) and (v_i', v_j'). The energy function is then expressed as:

$$E_{SR} = \sum_{(i,j)\in E} w_{ij} \left\| \left(v_i' - v_j'\right) - R_i(v_i - v_j) \right\|^2 \tag{10}$$

where $R_i \in SO(3)$ denotes the locally optimal rotation matrix at v_i, and $w_{ij} = \frac{1}{2}(cot\alpha_{ij} + cot\beta_{ij})$ represents the cotangent weight defined using the angles α_{ij} and β_{ij} opposite to edge (i, j) in its adjacent triangles.

The second energy term in Equation (9) serves as a soft constraint, enforcing the set of semantic structural points C from the original model to align to their target positions c_j. In the practical implementation of this study, however, to ensure strict alignment and stable preservation of semantic structural lines, hard positional constraints are imposed. Consequently, the deformed vertex positions are obtained by minimizing the energy E_{SR}:

$$\min_{\{v_j'\},\{R_i\}} \quad E_{SR} \quad \text{s.t.} \quad v_j' = c_j,\ j \in \mathcal{C} \tag{11}$$

E_{SR} is minimized by iteratively updating $\{R_i\}$ and $\{v_i'\}$ under the hard constraint of $v_j' = c_j$. In this way, we align the semantic structural lines of the original model with the regularized semantic structural lines to yield a structurally regularized building model (see Figures 2d and 3d), which provides a robust geometric foundation for the subsequent model simplification.

2.3. Edge Collapse Under Geometric Structural and Semantic Constraints

(1) Classical edge-collapse algorithm

The edge collapse simplification algorithm, originally proposed by Hoppe et al. [30], is one of the most widely used mesh simplification techniques in computer graphics and geometric modelling. The core idea is to determine whether two vertices in a mesh can be merged into a single new vertex based on an error cost metric to progressively reduce the number of vertices and faces while maintaining overall geometric fidelity. Following this idea, Garland and Heckbert proposed a QEM-based edge collapse algorithm [13], which has become the most commonly used and robust edge collapse simplification method. This approach determines the edge collapse order by constructing an error cost function based on the squared distances from a vertex to its adjacent planes. Let the plane equation of a triangular face be $ax + by + cz + d = 0$. For an arbitrary vertex point $p = [x, y, z, 1]^T$, its squared distance to the plane is given as follows:

$$\text{dist}(p) = \left(n^T p\right)^2 = p^T \left(nn^T\right) p \tag{12}$$

where $n = [a, b, c, d]^T$ is the homogeneous vector composed of the plane normal coefficients and the offset term, and the matrix $K = nn^T$ represents the quadratic form of the point-to-plane error.

For a vertex v, the QEM algorithm weights and accumulates the plane error matrices of its all adjacent triangular faces to obtain the overall error matrix Q_v as follows:

$$Q_v = \sum_k K_k = \sum_k n_k n_k^T \tag{13}$$

During the edge collapse process, the cost to merge two existing vertices on an edge $e_{ij} = (v_i, v_j)$ into a new vertex v' is calculated by summing up the two error matrices $Q = Q_i + Q_j$:

$$\Delta_{\text{collapse}} = v^T Q v \tag{14}$$

This error function is a quadratic form defined in homogeneous coordinates, representing the sum of squared distances between the collapsed vertex v' and the original set of planes. The optimal position of the new vertex v' after an edge collapse can be obtained by minimizing $\Delta_{collapse}$. Since $\Delta_{collapse}$ is a quadratic function, its minimization can be formulated as a convex problem. The optimal solution is obtained by solving $\frac{\partial \Delta}{\partial x} = \frac{\partial \Delta}{\partial y} = \frac{\partial \Delta}{\partial z} = 0$, such that $\Delta_{collapse}$ attains its minimum. This is equivalent to solving the following equation to find the optimal position of v':

$$\begin{bmatrix} q_{11} & q_{12} & q_{13} & q_{14} \\ q_{21} & q_{22} & q_{23} & q_{24} \\ q_{31} & q_{32} & q_{33} & q_{34} \\ 0 & 0 & 0 & 1 \end{bmatrix} v' = \begin{bmatrix} 0 \\ 0 \\ 0 \\ 1 \end{bmatrix} \tag{15}$$

If the coefficient matrix is invertible, then the optimal v' can be obtained by the following equation:

$$v' = \begin{bmatrix} q_{11} & q_{12} & q_{13} & q_{14} \\ q_{21} & q_{22} & q_{23} & q_{24} \\ q_{31} & q_{32} & q_{33} & q_{34} \\ 0 & 0 & 0 & 1 \end{bmatrix}^{-1} \begin{bmatrix} 0 \\ 0 \\ 0 \\ 1 \end{bmatrix} \tag{16}$$

Otherwise, the vertex with the minimum cost among v_i, v_j, and $\frac{v_i+v_j}{2}$ is selected. The main advantage of the QEM algorithm is using a unified error metric to quantify local geometric variations for efficient mesh simplification. However, it relies purely on geometric quadric errors and tends to overlook the importance of fine-grained structural components of building meshes, which can result in the loss of critical geometric details in complex 3D building models.

(2) Structural- and semantic-constrained edge collapse

To better preserve fine-grained structural details and critical semantic components of building models, we introduce an improved edge-collapse algorithm that integrates both the geometric structural constraints and architectural component semantic constraints. Our overall idea is to increase the collapse cost of edges associated with these regions of interest to preserve both the geometric details and the semantic integrity under high compression ratios. In the implementation, we do not directly use $\Delta_{collapse}$ derived from Equation (14) as the optimization metric. Instead, we apply separate weight amplification factors to the error matrices of the two vertices of each candidate edge. Let the edge to be collapsed be $e_{ij} = (v_i, v_j)$ and the corresponding vertex error matrices be Q_i and Q_j. First, we compute the weighting coefficients $w_{gs}(v_i)$ and $w_{gs}(v_j)$ for the two end vertices v_i and v_j. Then, the two matrices are scaled based on their weights and summed to obtain the weighted collapse cost of the edge at the current iteration.

$$\Delta_{gs}(v') = v'^T \left(\omega_{gs}(v_i)\, Q_i + \omega_{gs}(v_j)\, Q_j\right) v' \tag{17}$$

where $\Delta_{gs}(v_i)$ represents our proposed structural–semantic dual-constrained collapse cost. Intuitively, if an end vertex is identified as belonging to a geometric or semantic structural region, its error matrix contributes to Equation (17) with a larger weight. Thus, the associated cost of the corresponding edge is significantly increased to delay the collapse of this edge in the simplification priority queue. The weighting coefficient $w_{gs}(v)$ is jointly

determined by geometric saliency, normal inconsistency, and architectural component semantics, and is defined as follows:

$$\omega_{gs}(v) = \omega^N, \quad \text{where } N = I\big(G(v) \geq T_g\big) + I(\alpha_{\max} \geq T_a) + I(S(v) = 1) \tag{18}$$

where $I(\cdot)$ is an indicator function, which takes the value 1 if the condition is satisfied and 0 otherwise, w^N is a global factor to uniformly control the penalty strength of the geometric structural constraint and the semantic constraint, and N is the number of constraint conditions satisfied by the end vertices. We hypothesize that structural and semantic constraints are equally important in building model simplification. Thus, a uniform w is applied for both constraints. In our experiments, considering both structural preservation performance and geometric error control, w is set to 10. In practical applications, users can adjust its value according to user-defined requirements in order to adapt to different levels of structural component preservation of buildings.

The three terms in Equation (18) respectively represent:

- $I(G(v) \geq T_g)$: Geometric saliency. $G(v)$ represents the geometric saliency measure of vertex v, which is derived and normalized from Equation (5). If $G(v) \geq T_g$ with T_g set to 0.65 in the experiments, the vertex is considered to lie on ridge lines, corners, or other highly salient geometric structures. The indicator function takes the value 1, suggesting that the vertex should be preferentially preserved.
- $I(\alpha_{max} \geq T_\alpha)$: Normal inconsistency. α_{max} is the maximum angle deviation between the vertex normal and the normals of the incident faces in the one-ring neighbourhood of the vertex, indicating whether the local surface exhibits abrupt normal variations or potential flipping risks. When $\alpha_{max} \geq T_\alpha$ with T_α set to 60°, the indication function takes the value of 1 to prevent normal inversion or local surface collapse after edge simplification.
- $I(S(v) = 1)$: Building component semantics. $S(v)$ is a semantic indicator taking 1 when vertex v is an endpoint of a semantic structural line, and 0 otherwise. This term prioritizes the preservation of building-component semantic boundary lines during the edge-collapse process.

At the cost functions in Equations (17) and (18), the geometric structural constraint and the semantic constraint do not operate independently. They complementarily and mutually reinforce each other to regulate the edge-collapse cost. The structural constraint based on geometric saliency and normal inconsistency prevents the loss of local structural details and reduces the risk of triangle flipping, retaining edges in geometrically significant regions to better preserve local geometric details and morphological continuity under high compression ratios. In contrast, the building-component semantic constraint focuses on the semantic and structural relationships among building components. It avoids erroneous cross-component merging during the edge collapse, which improves the structural integrity and semantic interpretability of the simplified model at the component level. Collectively adopting both structural and semantic constraints enables the building model to maintain fine-grained structural details, component-level completeness, and enhanced semantic interpretability. Specifically, both constraints are integrated using a unified weight amplification mechanism. When the two vertices of a candidate edge simultaneously satisfy the structural and semantic constraints, the collapse cost of this edge is amplified exponentially as N increases. Collapse of such edges is greatly postponed in the priority queue, allowing edges that simultaneously show geometric details and component semantics to be effectively preserved. Compared with strategies based on linear weighting to a single constraint, our proposed dual-constraint penalty mechanism robustly prevents the loss of key structural regions, such as building ridges and component semantic boundaries, even under

extreme lightweighting conditions. Consequently, structural and semantic constraints are not only complementary at the information level but also collaboratively enhanced within the collapse-cost functions. By jointly optimizing the edge-collapse sequence under these constraints, the proposed method improves the overall quality of simplification results in terms of geometric accuracy and structural stability.

3. Results

3.1. Dataset of Building Models

To comprehensively evaluate the effectiveness of our approach under dual constraints of geometric structure and building component semantics, we organized the experimental datasets according to the applicability of different constraints. A progressive evaluation was performed, starting from validating the method's capability to preserve geometric structural details and extending to an overall assessment of model simplification performance under both constraints in complex scenarios.

We first focused on structural degradation that commonly occurs during building model simplification, such as the loss of detailed architectural features and triangle normal flipping issues. To validate whether our proposed geometric structural constraint based on geometric saliency and normal inconsistency can effectively alleviate these issues, we randomly selected 40 individual building models from the public platform Sketchfab [50] and categorized them into two groups: modern architectural geometric models and cultural heritage building models. In this experiment, we only activated the geometric structural constraint. The building models have diverse shapes, sizes, and architectural styles, and do not contain semantic annotations. Among them, 21 modern building models exhibit regular structures and well-defined boundaries, while the remaining 19 cultural heritage building models generally contain complex curvature variations. Thus, the dataset serves as a sufficient data source for evaluating the proposed geometric structural constraint under various levels of structural complexity.

To evaluate the effectiveness of the geometric structural constraint in preserving global structural relationships on large-scale urban buildings, we selected two city-level building datasets reconstructed from real urban scenes, SUM [51] and STPLS3D [52]. SUM is a high-resolution mesh model of a complex urban area of approximately 4 km^2 in Helsinki, Finland, reconstructed using aerial oblique imagery and ContextCapture. It provides semantic annotations on both point clouds and meshes containing six classes (e.g., terrain, buildings, and high vegetation). Similar to SUM, STPLS3D was also reconstructed using ContextCapture. However, it covers an area exceeding 17 km^2 which includes both real and synthetic scenes. The real-scene mesh models contain six categories of outdoor urban semantics, including ground, buildings, trees, vehicles, lamp posts, and fences. Based on SUM and STPLS3D, we extracted building meshes with architectural semantic labels for subsequent model simplification. Both datasets have a massive volume of triangles, diverse architectural shapes, and significant local noise, which can be challenging to tackle. Employing only the geometric constraint allows us to clearly evaluate the scalability of the proposed structural-constrained edge-collapse strategy in large urban scenes, as well as its capability to preserve global urban structural morphology and local geometric details.

To further enhance the preservation of key building components and semantic boundaries, we incorporate building semantic constraints. Semantic structural lines reflect component-level structures of buildings such as ridges, wall transitions, and roof regions. This semantic information provides component-level structural cues beyond local geometry, enabling more informed edge-collapse decisions. In this experiment, we used the semantic point clouds provided by ArCH [41] to evaluate the effectiveness of the proposed semantics-aware constraint. The dataset contains high-resolution point clouds of

17 historical building scenes acquired by close-range photogrammetry and laser scanning, with nine semantic classes included (i.e., walls, floor, roof, column, moldings, vault, arch, stair, window/door). This data does not provide corresponding 3D mesh models. However, we could use the Poisson reconstruction method to obtain dense building mesh models that preserve both the geometric shapes and building-component semantic boundaries. Therefore, Arch provides ideal experimental data for validating the effectiveness of our method on complex building models. On the ArCH dataset, the geometric structural constraint and the semantic component constraint are jointly used to evaluate our method from aspects of semantic structure preservation, semantic boundary completeness, and postponed collapse of important components for fine-detail protection.

We adopted various levels of compression ratios to fairly compare experimental results on different datasets and under different constraint configurations. Two geometric accuracy metrics, Root Mean Square Error (RMSE) and Mean Absolute Error (MAE), are used for quantitative evaluations. These metrics are computed between the final simplified model and the original mesh prior to deformation. Therefore, any geometric deviation introduced by the Laplacian deformation step is naturally included in the reported error metrics.

MAE represents the average absolute deviation between the simplified building model and the original model. It can be used to estimate the overall error and is calculated as follows:

$$\mathrm{MAE} = \frac{1}{n}\sum_{i=1}^{n}|d(p_i, \hat{p}_i)| \tag{19}$$

where n is the total number of vertices, p_i is the i^{th} vertex position on the simplified mesh, $\hat{p}_i$ is its closest vertex position on the original mesh, and $d(p_i, \hat{p}_i)$ represents the Euclidean distance between the two vertices.

RMSE measures the root mean squared deviation between the simplified mesh and the original mesh. Compared to MAE, it emphasizes the influence of large errors and thus is more sensitive to extreme deviations. RMSE is computed as follows:

$$\mathrm{RMSE} = \sqrt{\frac{1}{n}\sum_{i=1}^{n}(d(p_i, \hat{p}_i))^2} \tag{20}$$

3.2. Single-Building Model Simplification Under Geometric Structural Constraint

We randomly selected 40 models from the Sketchfab [50] open data platform to evaluate the effectiveness of the geometric structural constraint, in comparison with methods of GH [13], LT [31], and SLA [37]. As shown in Figure 4, as the simplification ratio of the *Heritage_5* model increases, all methods exhibit a stable increase. Compared to the rest of the methods, our method consistently achieves the lowest error rates across all compression ratios, demonstrating the effectiveness and superiority of the proposed geometric structural constraint in preserving building geometric structure details. Figures 5–7 illustrate local structural detail comparisons of GH, LT, and SLA at a compression ratio of 10%.

For the 21 modern building models in Sketchfab, we uniformly adopted a compression ratio of 10% for all methods to ensure a fair comparison. The quantitative results are reported in Tables 1 and 2, while the corresponding visual simplification results for modern buildings under a compression ratio of 10% are shown in Figures 8–10. As modern buildings predominantly contain planar surfaces, straight ridge lines, and regular-shaped facades, it is easy to recognize structural discontinuities by evaluating the geometric saliency and local normal variation. Incorporating the geometric structural constraint better captures the principal geometric structural lines of buildings and effectively avoids the fine structural loss that occurs in the GH method. This was verified in Tables 1 and 2, where our method based on the geometric structural constraint achieves low RMSE and MAE on all the

models. In general, its errors are lower than or comparable to those of the GH method, and are clearly superior to those of the LT and SLA methods, indicating that our method robustly preserves the overall building structural patterns. Especially for models with ridges, roof transitions, or highly curvy regions (e.g., the window in Figure 5a, the terrace railing in Figure 6b, and the lightning rod in Figure 7b), incorporating the geometric structural constraint significantly reduces local shape distortions in the simplified models. Among all the modern building models with varying structural complexities, our method achieves higher simplification accuracy than other methods for most models under the same compression ratio, demonstrating that enforcing the geometric structural constraint based on local saliency and normal inconsistency robustly reduces geometric errors during the edge-collapse process.

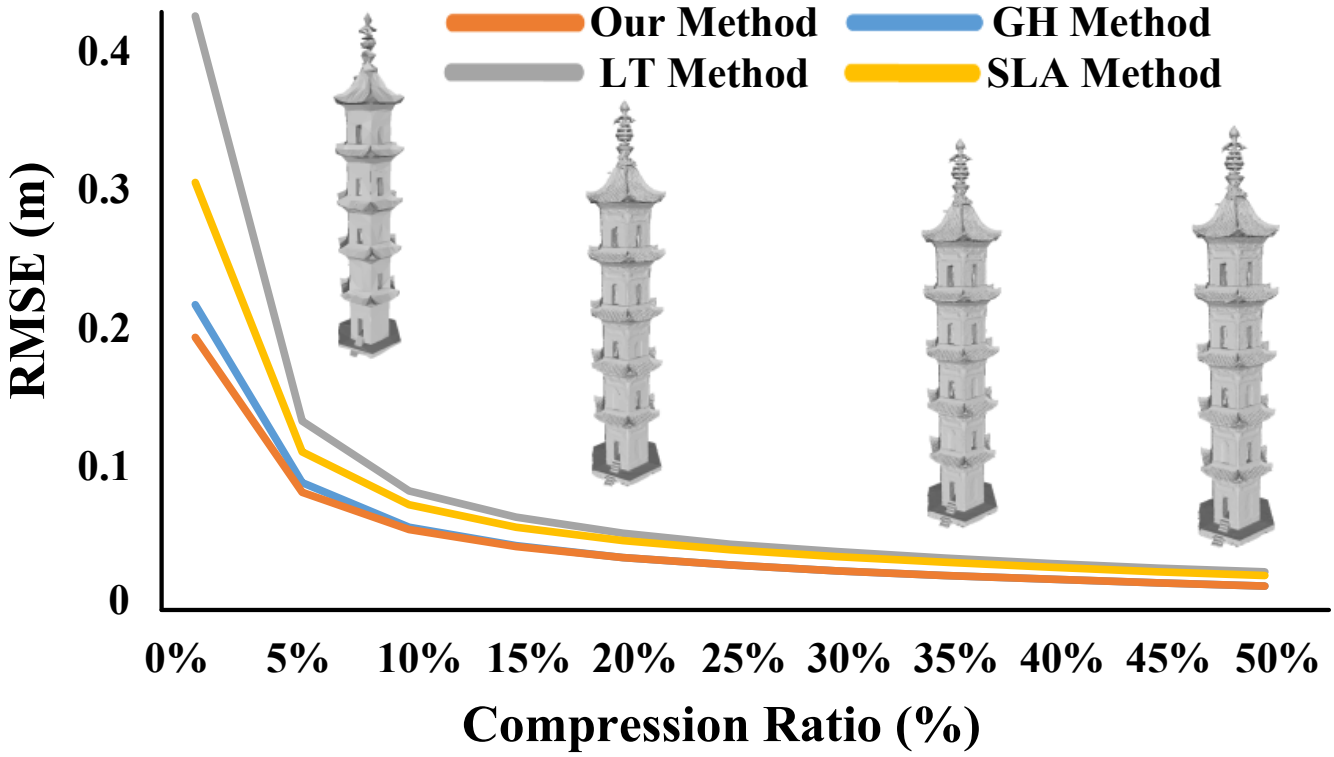

Figure 4. Comparison of RMSE trends of different simplification methods with respect to compression ratio on the Heritage_5 building model from Sketchfab. The horizontal axis denotes the model compression ratio, and the vertical axis denotes RMSE (m). The curves correspond to GH, LT, SLA, and the proposed method. Simplification results under compression ratios of 1%, 10%, 30%, and 50% are presented from left to right.

Compared with modern building models, cultural heritage building models are by nature more complex, exhibiting multi-level components, densely distributed fine structures, and curvature variations. As shown in Tables 3 and 4, to more comprehensively evaluate the performance of geometric structural constraints, we performed experiments on 19 cultural heritage building models from Sketchfab using three simplification ratios (30%, 10%, and 1%), with the corresponding visual results under a compression ratio of 10% presented in Figures 11–13. Results indicate that at ratios of 30% and 10%, the performances of our method and of the GH method are similar. However, our method exhibits a slightly more stable performance. When the compression ratio is reduced to 1%, the error rate of the GH method greatly increases for most cultural heritage models, showing a tendency toward structural collapse, as illustrated in Figure 5d. For the LT method, errors on structurally complex heritage models are mainly volumetric expansion or shrinkage in

detailed components (Figure 6d), where the upturned eaves are excessively sharpened, and smaller ridge ornaments become severely contracted. In contrast, our method, enhanced with the geometric structural constraint, demonstrates a slower error increase and is able to preserve more complete structural features under significant compression, particularly in regions with high curvature and complex geometric transitions.

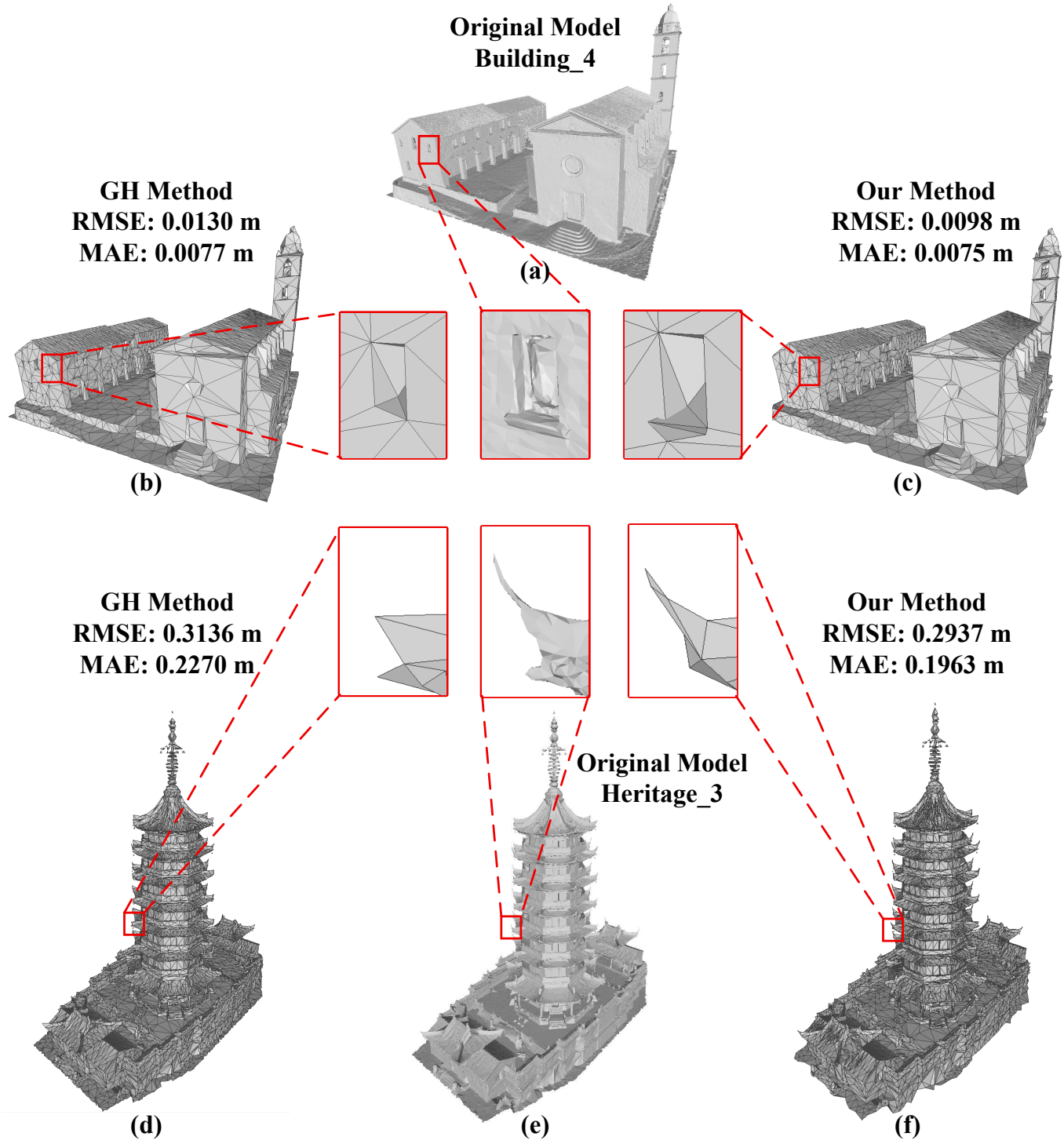

Figure 5. Visual comparison of structural detail preservation between the GH method and the proposed geometric structural constraint method under a compression ratio of 10%. Subfigures (**a**,**e**) present the original models of Building_4 and Heritage_3 from Sketchfab. Subfigures (**b**,**d**) show the simplification results produced by the GH method. Subfigures (**c**,**f**) illustrate the simplification results obtained by the proposed method.

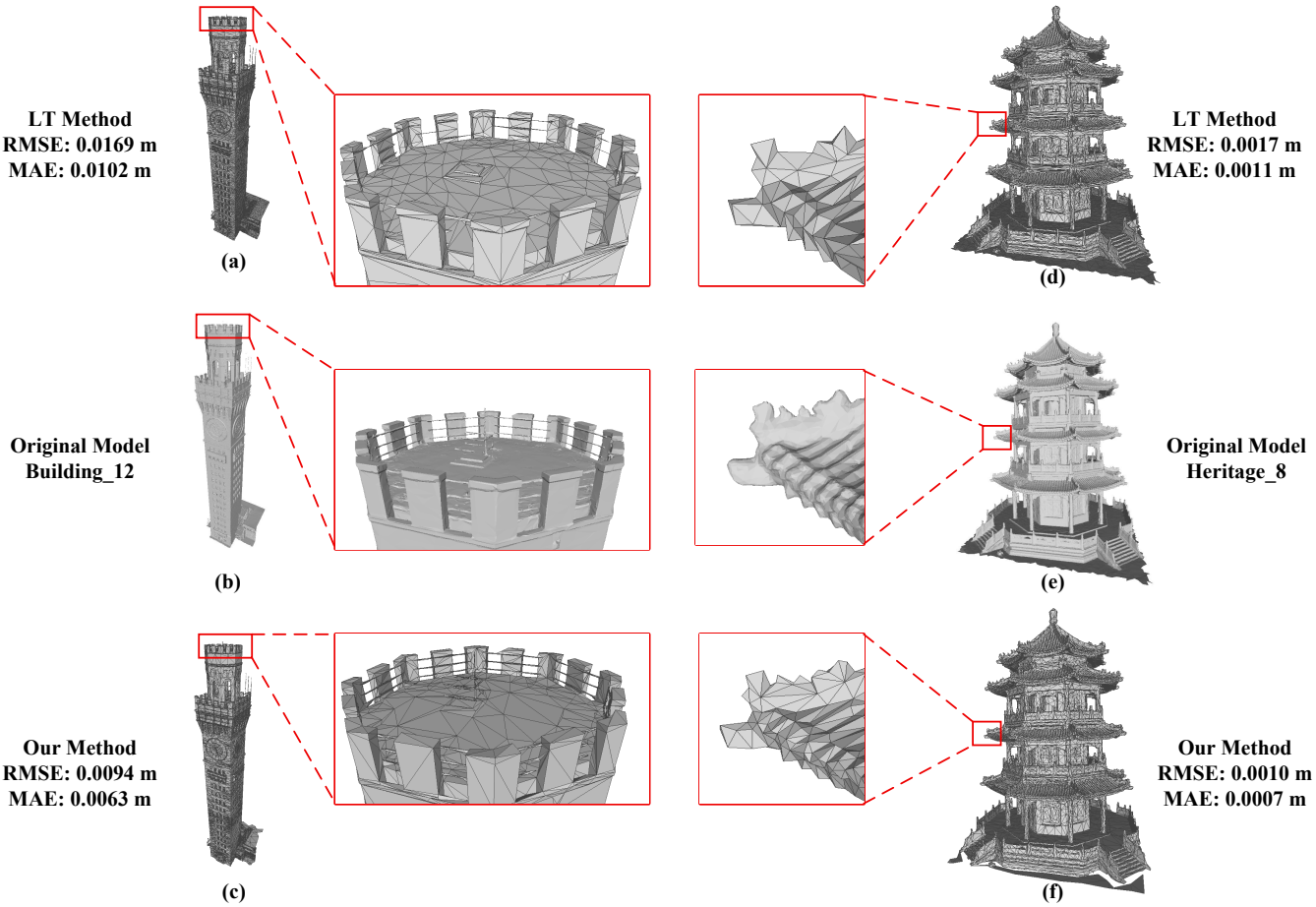

Figure 6. Visual comparison of structural detail preservation between the LT method and the proposed geometric structural constraint method under a compression ratio of 10%. Subfigures (**b**,**e**) present the original models of Building_12 and Heritage_8 from Sketchfab. Subfigures (**a**,**d**) show the simplification results produced by the LT method. Subfigures (**c**,**f**) illustrate the simplification results obtained by the proposed method.

On both modern and cultural heritage building models, our geometric-structural constrained method shows stable performance gains compared to the other methods. This is due to the effectiveness of the geometric saliency metric in identifying local geometric features and high-curvature regions, which allows the edge collapse procedure to preferentially preserve critical structural elements. In addition, the normal inconsistency metric mitigates face flipping and local shape distortion. For both model categories, our proposed method yields lower and more stable RMSE and MAE values with reduced variance, indicating a stronger generalizability to different architectural styles.

Compared with the LT and SLA methods, our method can preserve more complete fine structures of buildings with improved geometric accuracy. It should be noted, however, that for a few building models, GH achieves RMSE values that are comparable to or slightly lower than those of our method. Such cases typically occur in models with highly regular geometric shapes, which can make our algorithm insensitive to the edge collapse order. Still, in these cases, the performance differences are marginal. For most models, our method exhibits a significant performance improvement compared to the GH method.

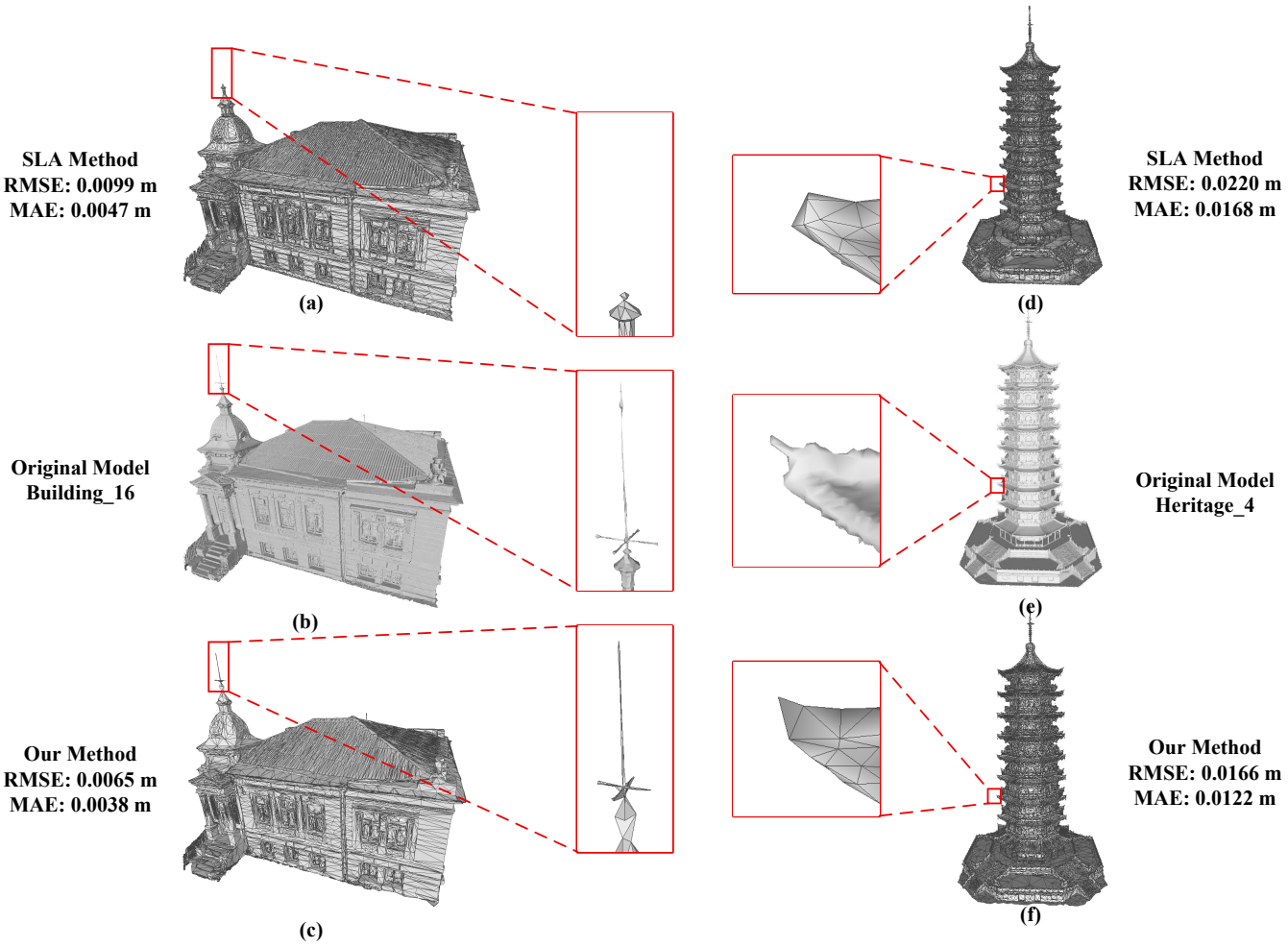

Figure 7. Visual comparison of structural detail preservation between the SLA method and the proposed geometric structural constraint method under a compression ratio of 10%. Subfigures (**b**,**e**) present the original models of Building_16 and Heritage_4 from Sketchfab. Subfigures (**a**,**d**) show the simplification results produced by the SLA method. Subfigures (**c**,**f**) illustrate the simplification results obtained by the proposed method.

3.3. City-Scale Building Model Simplification Under Geometric Structural Constraint

Compared with individual building models, large-scale city-level building models are significantly more complex, exhibiting high variance in size and shape, roof discontinuities, irregular geometric structures, and data noise. It is necessary to consider not only the structural edges of individual buildings but also the relationships among continuous surface patches spanning multiple buildings. Furthermore, it is very likely to introduce artefacts such as misaligned structural edges, local shape collapse, and erroneous flipping of surface patches in the simplification process. Such scenarios provide a more rigorous evaluation of the stability and generalizability of the proposed geometric structural constrained method in large-scale scenes. Based on two city-level building model datasets SUM and STPLS3D, we compared our method and three simplification approaches, GH, LT, and SLA, under a simplification ratio of 10%. The quantitative results are reported in Table 5. The visual results obtained with the geometric structural constraint are illustrated in Figure 14.

Table 1. Quantitative comparison of the proposed geometric structural constraint method with GH, LT, and SLA on 21 modern building models from Sketchfab under a compression ratio of 10%. RMSE and MAE are reported for evaluation. In this table, we report the first part of the results for Building_1 to Building_10. The remaining results for Building_11 to Building_21 are presented in Table 2.

Model	Initial Vertex #	Result Vertex #	RMSE (m)	MAE (m)	Comparative Methods
Building_1	334,449	33,249	0.0966	0.0733	GH
			0.1714	0.1127	LT
			0.1365	0.0943	SLA
			0.0958	0.0681	Ours
Building_2	42,659	4345	0.0005	0.0004	GH
			0.0006	0.0004	LT
			0.0006	0.0004	SLA
			0.0004	0.0003	Ours
Building_3	120,307	12,026	0.5058	0.3908	GH
			0.8215	0.5508	LT
			1.5638	0.5287	SLA
			0.5218	0.3553	Ours
Building_4	332,079	33,194	0.0103	0.0077	GH
			0.0143	0.0097	LT
			0.0124	0.0089	SLA
			0.0098	0.0075	Ours
Building_5	311,990	31,025	0.0017	0.0013	GH
			0.0026	0.0016	LT
			0.0022	0.0016	SLA
			0.0016	0.0011	Ours
Building_6	311,400	31,415	0.0059	0.0042	GH
			0.0079	0.0051	LT
			0.0164	0.0050	SLA
			0.0053	0.0040	Ours
Building_7	334,655	32,051	0.0110	0.0082	GH
			0.0172	0.0113	LT
			0.0302	0.0098	SLA
			0.0104	0.0077	Ours
Building_8	337,866	33,425	0.0112	0.0084	GH
			0.0163	0.0112	LT
			0.0146	0.0101	SLA
			0.0107	0.0080	Ours
Building_9	295,032	29,498	0.0081	0.0062	GH
			0.0106	0.0074	LT
			0.0092	0.0067	SLA
			0.0079	0.0060	Ours
Building_10	178,424	17,964	0.0058	0.0042	GH
			0.0079	0.0052	LT
			0.0107	0.0051	SLA
			0.0053	0.0040	Ours

Table 2. Quantitative comparison of the proposed geometric structural constraint method with GH, LT, and SLA on 21 modern building models from Sketchfab under a compression ratio of 10%. RMSE and MAE are reported for evaluation. In this table, we report the first part of the results for Building_11 to Building_21. The remaining results for Building_1 to Building_10 are presented in Table 1.

Model	Initial Vertices #	Result Vertices #	RMSE (m)	MAE (m)	Comparative Methods
Building_11	501,812	50,302	0.0044	0.0034	GH
			0.0071	0.0049	LT
			0.0061	0.0046	SLA
			0.0044	0.0033	Ours
Building_12	472,417	46,244	0.0091	0.0069	GH
			0.0169	0.0102	LT
			0.0118	0.0086	SLA
			0.0094	0.0063	Ours
Building_13	500,203	49,825	0.0028	0.0021	GH
			0.0045	0.0028	LT
			0.0036	0.0025	SLA
			0.0027	0.0018	Ours
Building_14	268,134	26,983	0.0005	0.0004	GH
			0.0009	0.0005	LT
			0.0011	0.0005	SLA
			0.0005	0.0003	Ours
Building_15	769,965	75,833	0.0032	0.0025	GH
			0.0051	0.0034	LT
			0.0041	0.0030	SLA
			0.0032	0.0023	Ours
Building_16	281,076	22,481	0.0071	0.0043	GH
			0.0103	0.0057	LT
			0.0099	0.0047	SLA
			0.0065	0.0038	Ours
Building_17	482,478	47,766	0.0098	0.0075	GH
			0.0156	0.0103	LT
			0.0131	0.0092	SLA
			0.0097	0.0074	Ours
Building_18	398,001	39,890	0.0024	0.0018	GH
			0.0037	0.0024	LT
			0.0035	0.0024	SLA
			0.0024	0.0016	Ours
Building_19	266,744	26,427	0.0109	0.0079	GH
			0.0151	0.0100	LT
			0.0148	0.0091	SLA
			0.0103	0.0075	Ours
Building_20	238,953	23,904	0.6946	0.5122	GH
			1.0360	0.6688	LT
			1.0331	0.6633	SLA
			0.6928	0.4555	Ours
Building_21	265,618	28,935	0.0002	0.0001	GH
			0.0002	0.0001	LT
			0.0003	0.0002	SLA
			0.0001	0.0001	Ours

Table 3. Quantitative comparison of the proposed geometric structural constraint method with GH, LT, and SLA on 19 cultural heritage building models from Sketchfab under compression ratios of 30%, 10%, and 1%. RMSE and MAE are reported for evaluation. In this table, we report the first part of the results for Heritage_1 to Heritage_10. The remaining results for Heritage_11 to Heritage_19 are presented in Table 4.

Model	Compression Ratio 30%		Compression Ratio 10%		Compression Ratio 1%		Comparative Methods
	RMSE (m)	MAE (m)	RMSE (m)	MAE (m)	RMSE (m)	MAE (m)	
Heritage_1	0.0477	0.0364	0.0968	0.0740	0.4130	0.3055	GH
	0.0801	0.0500	0.1709	0.1133	0.7551	0.5163	LT
	0.0799	0.0449	0.1534	0.0974	0.5412	0.3718	SLA
	0.0487	0.0356	0.0938	0.0709	0.3811	0.2741	Ours
Heritage_2	0.0277	0.0210	0.0576	0.0425	0.2604	0.1819	GH
	0.0410	0.0264	0.0877	0.0574	0.3920	0.2251	LT
	0.0618	0.0253	0.1146	0.0563	0.3741	0.2019	SLA
	0.0276	0.0207	0.0549	0.0408	0.1951	0.1443	Ours
Heritage_3	0.0356	0.0273	0.0734	0.0560	0.3136	0.2270	GH
	0.0612	0.0378	0.1316	0.0858	0.5824	0.3867	LT
	0.1067	0.0342	0.1910	0.0739	0.6237	0.2766	SLA
	0.0356	0.0262	0.0722	0.0531	0.2937	0.1963	Ours
Heritage_4	0.0083	0.0064	0.0166	0.0129	0.0622	0.0467	GH
	0.0143	0.0090	0.0317	0.0200	0.1019	0.0712	LT
	0.0116	0.0079	0.0229	0.0168	0.0717	0.0548	SLA
	0.0083	0.0061	0.0166	0.0122	0.0559	0.0366	Ours
Heritage_5	0.0267	0.0206	0.0564	0.0439	0.2088	0.1644	GH
	0.0397	0.0267	0.0812	0.0579	0.4065	0.2792	LT
	0.0364	0.0254	0.0719	0.0539	0.2924	0.2168	SLA
	0.0267	0.0204	0.0557	0.0402	0.1864	0.1428	Ours
Heritage_6	0.0269	0.0202	0.0612	0.0451	0.2895	0.1982	GH
	0.0466	0.0277	0.0944	0.0618	0.5277	0.3264	LT
	0.0401	0.0245	0.0778	0.0540	0.2838	0.2023	SLA
	0.0271	0.0191	0.0557	0.0401	0.2731	0.1706	Ours
Heritage_7	0.0004	0.0003	0.0011	0.0008	0.0087	0.0049	GH
	0.0006	0.0004	0.0017	0.0011	0.0101	0.0067	LT
	0.0006	0.0004	0.0015	0.0010	0.0068	0.0050	SLA
	0.0004	0.0003	0.0010	0.0007	0.0046	0.0035	Ours
Heritage_8	0.0037	0.0029	0.0087	0.0066	0.0484	0.0323	GH
	0.0058	0.0036	0.0139	0.0094	0.0535	0.0366	LT
	0.0054	0.0034	0.0122	0.0088	0.0436	0.0316	SLA
	0.0038	0.0028	0.0084	0.0064	0.0338	0.0241	Ours
Heritage_9	0.0023	0.0017	0.0052	0.0041	0.0233	0.0175	GH
	0.0034	0.0022	0.0079	0.0055	0.0363	0.0244	LT
	0.0031	0.0021	0.0070	0.0052	0.0300	0.0221	SLA
	0.0030	0.0017	0.0063	0.0041	0.0227	0.0171	Ours
Heritage_10	0.0017	0.0013	0.0036	0.0028	0.0117	0.0082	GH
	0.0027	0.0018	0.0055	0.0039	0.0174	0.0114	LT
	0.0024	0.0017	0.0047	0.0035	0.0134	0.0099	SLA
	0.0016	0.0012	0.0035	0.0027	0.0112	0.0075	Ours

Table 4. Quantitative comparison of the proposed geometric structural constraint method with GH, LT, and SLA on 19 cultural heritage building models from Sketchfab under compression ratios of 30%, 10%, and 1%. RMSE and MAE are reported for evaluation. In this table, we report the first part of the results for Heritage_11 to Heritage_19. The remaining results for Heritage_1 to Heritage_10 are presented in Table 3.

Model	Compression Ratio 30%		Compression Ratio 10%		Compression Ratio 1%		Comparative Methods
	RMSE (m)	MAE (m)	RMSE (m)	MAE (m)	RMSE (m)	MAE (m)	
Heritage_11	0.0085	0.0048	0.0326	0.0194	0.0693	0.0241	GH
	0.0084	0.0050	0.0181	0.0117	0.0724	0.0450	LT
	0.0118	0.0060	0.0391	0.0194	0.0359	0.0248	SLA
	0.0086	0.0047	0.0326	0.0186	0.0711	0.0243	Ours
Heritage_12	0.0028	0.0022	0.0051	0.0039	0.0167	0.0118	GH
	0.0036	0.0026	0.0063	0.0045	0.0220	0.0145	LT
	0.0032	0.0025	0.0053	0.0041	0.0196	0.0140	SLA
	0.0027	0.0021	0.0042	0.0033	0.0118	0.0084	Ours
Heritage_13	0.0087	0.0062	0.0188	0.0143	0.0768	0.0509	GH
	0.0137	0.0077	0.0257	0.0167	0.0934	0.0621	LT
	0.0109	0.0067	0.0218	0.0154	0.0772	0.0488	SLA
	0.0086	0.0061	0.0187	0.0141	0.0736	0.0483	Ours
Heritage_14	0.0018	0.0013	0.0045	0.0033	0.0184	0.0135	GH
	0.0027	0.0016	0.0060	0.0040	0.0247	0.0166	LT
	0.0023	0.0014	0.0053	0.0039	0.0215	0.0159	SLA
	0.0018	0.0012	0.0042	0.0029	0.0173	0.0113	Ours
Heritage_15	0.0058	0.0044	0.0129	0.0095	0.0534	0.0377	GH
	0.0092	0.0059	0.0179	0.0127	0.0804	0.0555	LT
	0.0079	0.0054	0.0154	0.0116	0.0619	0.0446	SLA
	0.0058	0.0038	0.0117	0.0078	0.0407	0.0268	Ours
Heritage_16	0.0006	0.0005	0.0013	0.0010	0.0059	0.0044	GH
	0.0010	0.0007	0.0023	0.0016	0.0091	0.0065	LT
	0.0009	0.0006	0.0019	0.0014	0.0062	0.0047	SLA
	0.0005	0.0004	0.0013	0.0010	0.0053	0.0039	Ours
Heritage_17	0.0067	0.0051	0.0163	0.0123	0.1059	0.0628	GH
	0.0108	0.0067	0.0239	0.0166	0.0994	0.0691	LT
	0.0103	0.0065	0.0216	0.0157	0.0921	0.0685	SLA
	0.0111	0.0051	0.0151	0.0119	0.0617	0.0465	Ours
Heritage_18	0.0020	0.0015	0.0042	0.0032	0.0164	0.0188	GH
	0.0031	0.0020	0.0064	0.0043	0.0217	0.0148	LT
	0.0028	0.0019	0.0057	0.0042	0.0927	0.0685	SLA
	0.0019	0.0014	0.0041	0.0031	0.0140	0.0103	Ours
Heritage_19	0.4337	0.3137	1.3116	1.0276	6.3987	4.9691	GH
	0.6811	0.3958	1.8923	1.2810	9.6720	6.7482	LT
	0.6215	0.3835	1.7348	1.2596	8.3101	6.2475	SLA
	0.4482	0.3138	1.3255	1.2058	6.3144	4.8819	Ours

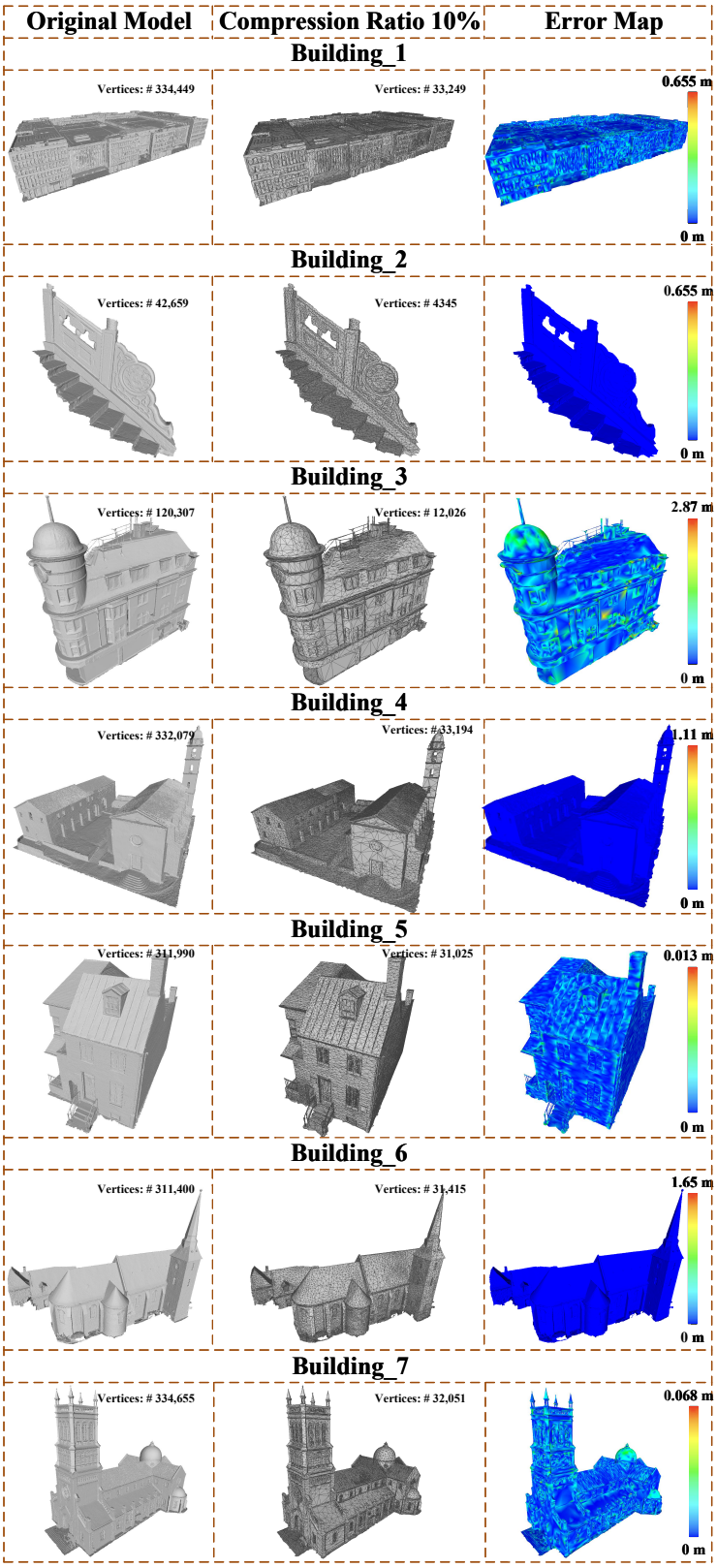

Figure 8. Simplification results of 21 modern building mesh models from Sketchfab using the proposed geometric structural constraint method under a compression ratio of 10%. From left to right, the original model, the simplified model at 10% compression, and the corresponding geometric error map are presented. In this figure, we visualize the first part of the results for Building_1 to Building_7. The results for Building_8 to Building_14 and Building_15 to Building_21 are presented in Figure 9 and Figure 10, respectively.

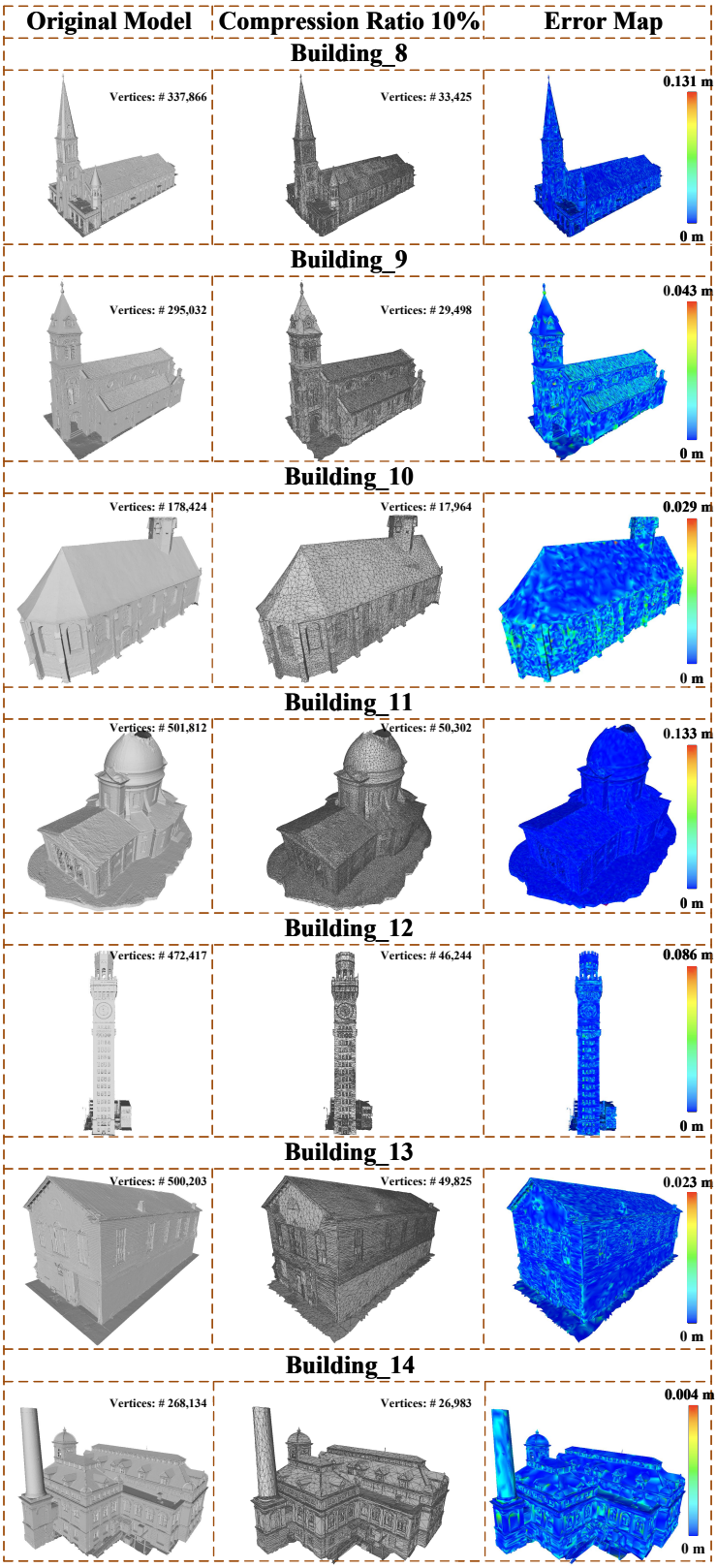

Figure 9. Simplification results of 21 modern building mesh models from Sketchfab using the proposed geometric structural constraint method under a compression ratio of 10%. From left to right, the original model, the simplified model at 10% compression, and the corresponding geometric error map are presented. In this figure, we visualize the first part of the results for Building_8 to Building_14. The results for Building_1 to Building_7 and Building_15 to Building_21 are presented in Figure 8 and Figure 10, respectively.

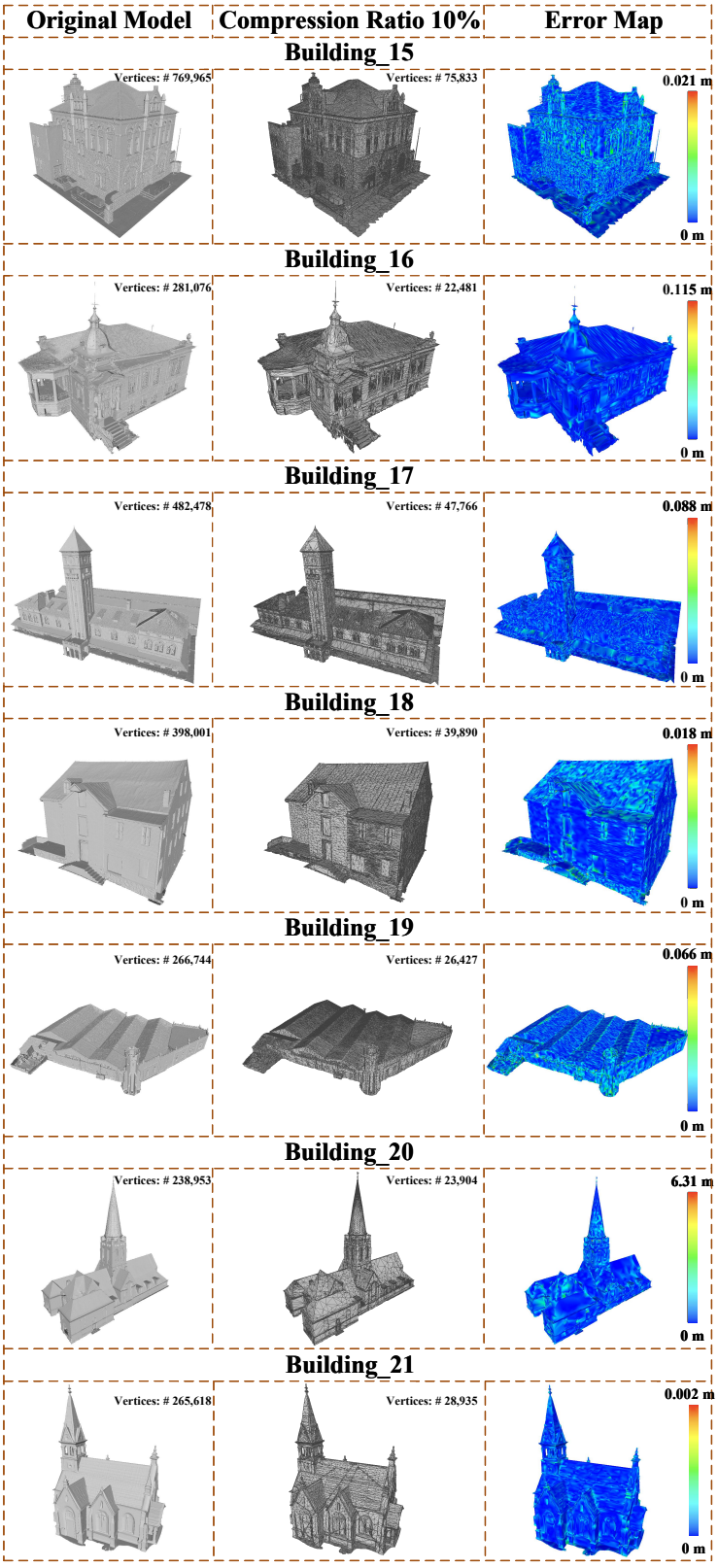

Figure 10. Simplification results of 21 modern building mesh models from Sketchfab using the proposed geometric structural constraint method under a compression ratio of 10%. From left to right, the original model, the simplified model at 10% compression, and the corresponding geometric error map are presented. In this figure, we visualize the first part of the results for Building_15 to Building_21. The results for Building_1 to Building_7 and Building_8 to Building_14 are presented in Figure 8 and Figure 9, respectively.

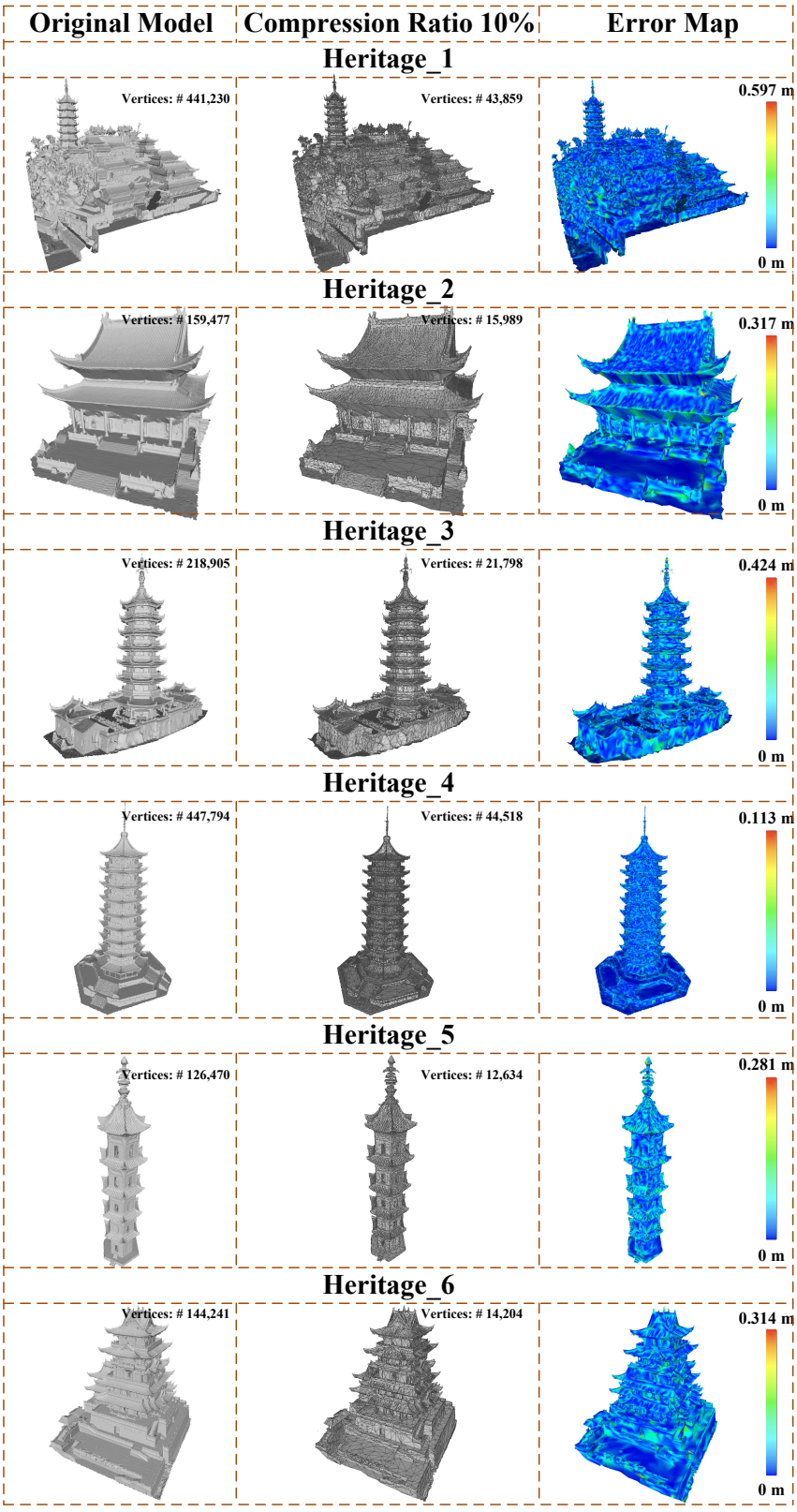

Figure 11. Simplification results of 19 cultural heritage building mesh models from Sketchfab using the proposed geometric structural constraint method under a compression ratio of 10%. From left to right, the original model, the simplified model at 10% compression, and the corresponding geometric error map are presented. In this figure, we visualize the first part of the results for Heritage_1 to Heritage_6. The results for Heritage_7 to Heritage_12 and Heritage_13 to Heritage_19 are presented in Figure 12 and Figure 13, respectively.

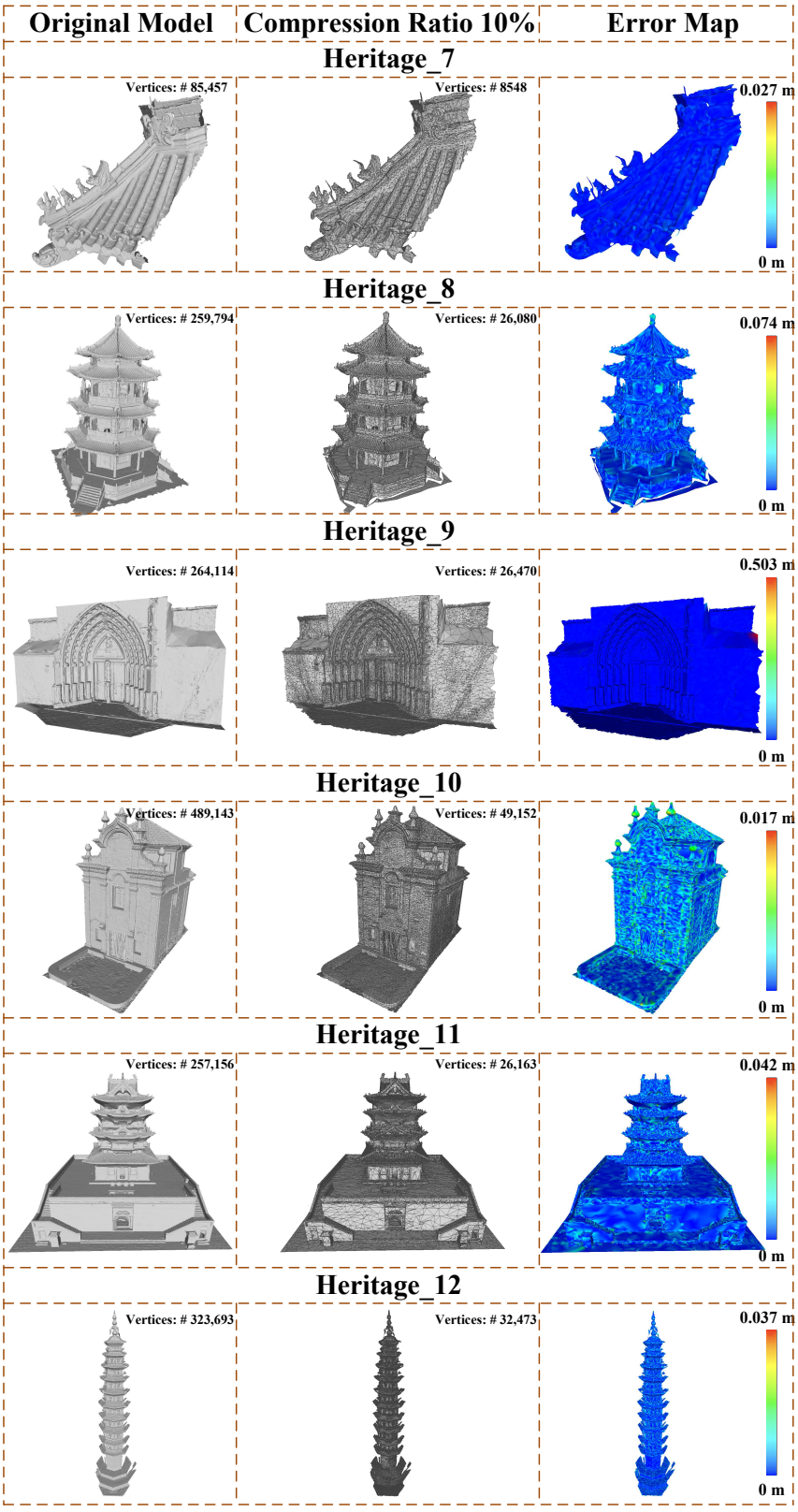

Figure 12. Simplification results of 19 cultural heritage building mesh models from Sketchfab using the proposed geometric structural constraint method under a compression ratio of 10%. From left to right, the original model, the simplified model at 10% compression, and the corresponding geometric error map are presented. In this figure, we visualize the first part of the results for Heritage_7 to Heritage_12. The results for Heritage_1 to Heritage_6 and Heritage_13 to Heritage_19 are presented in Figure 11 and Figure 13, respectively.

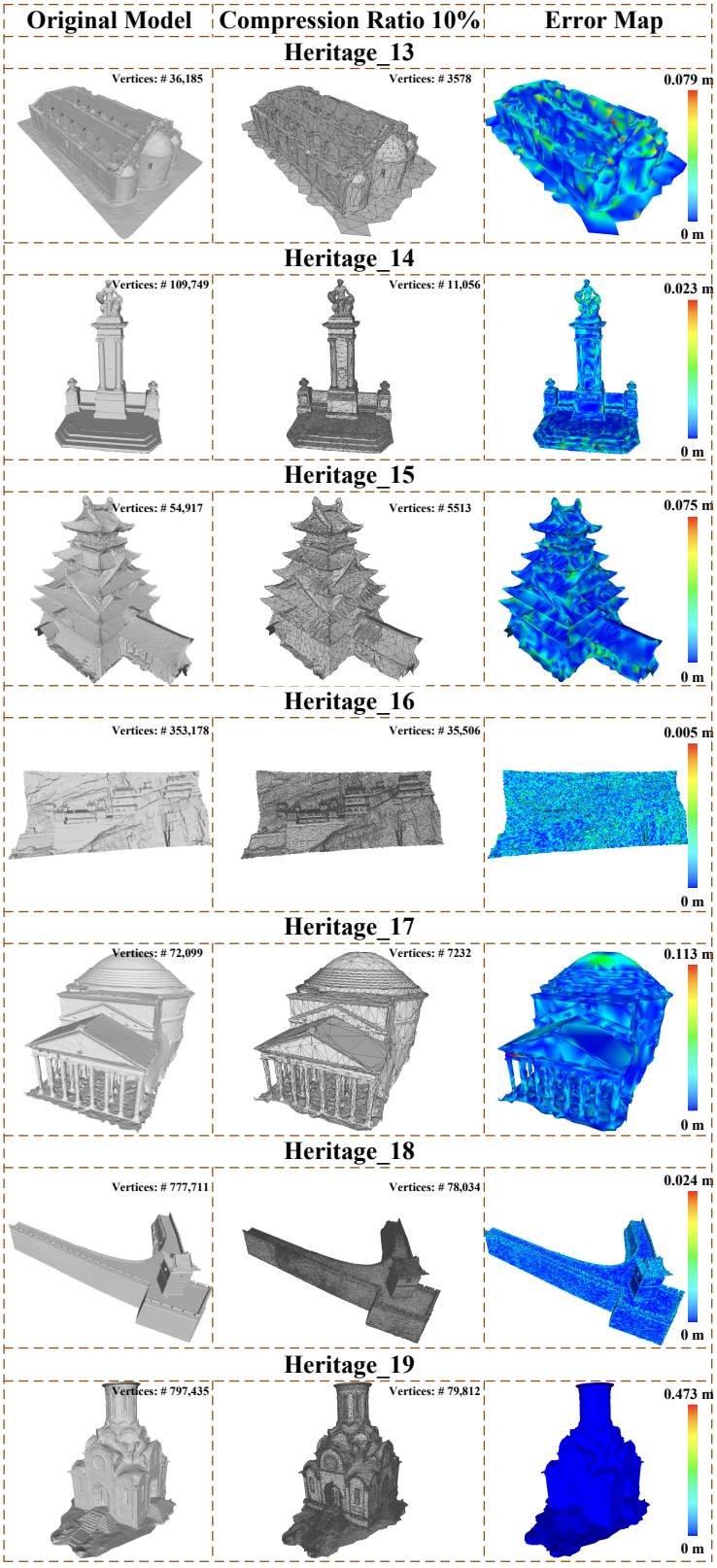

Figure 13. Simplification results of 19 cultural heritage building mesh models from Sketchfab using the proposed geometric structural constraint method under a compression ratio of 10%. From left to right, the original model, the simplified model at 10% compression, and the corresponding geometric error map are presented. In this figure, we visualize the first part of the results for Heritage_13 to Heritage_19. The results for Heritage_1 to Heritage_6 and Heritage_7 to Heritage_12 are presented in Figure 11 and Figure 12, respectively.

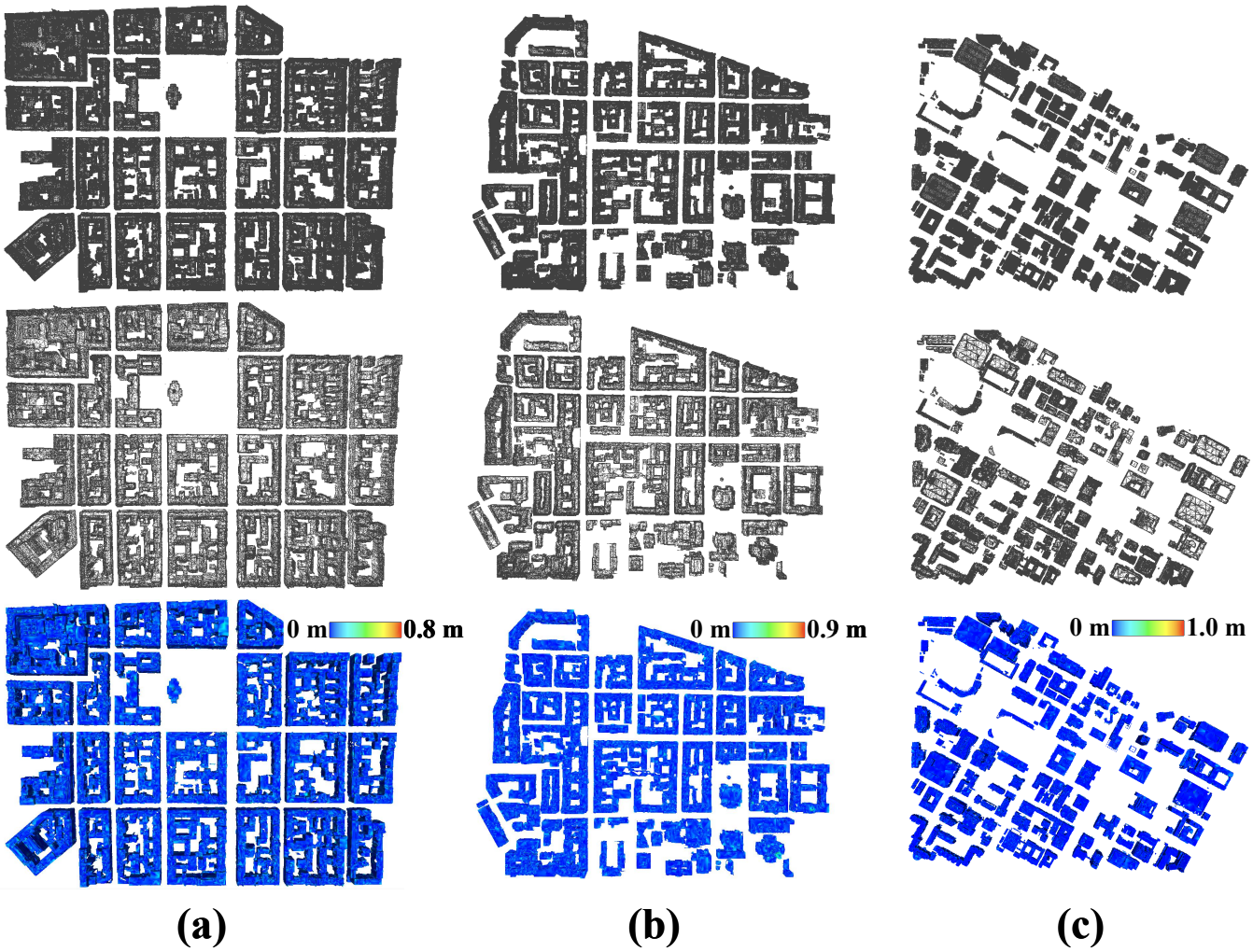

Figure 14. Simplification results of large-scale urban-level building models via the proposed geometric structure constrained method with a compression ratio of 10%. Subfigure (**a**) presents the Part 1 area of the SUM dataset, (**b**) the Part 2 area of the SUM dataset, and (**c**) the USC area of the STPLS3D dataset. From top to bottom, the original model, the simplified model at 10% compression, and the corresponding geometric error map are shown.

Overall, our method demonstrates stable and substantial error reduction across all city-scale models. For the two regions in the SUM dataset (SUM Part1 and SUM Part2), the GH method yields RMSE values of 0.1131 m and 0.1125 m, while our method reduces them to 0.0990 m and 0.0975 m, reducing the errors to approximately 1214%. The MAE values of our method are also decreased from 0.0855 m and 0.0847 m to 0.0754 m and 0.0738 m, respectively. The LT method produces RMSE values of 0.1650 m and 0.1705 m, which are obviously higher than those of both the GH method and our method. This indicates that, in dense and complex urban-scale scenes, the lack of explicit geometric structural constraints makes it difficult to prevent the cumulative propagation of collapse errors and can lead to the degradation of salient structural features. The SLA method achieves an RMSE of 0.1413 m in SUM Part1 and 0.1033 m in SUM Part2. Although it outperforms the GH method in certain regions, its geometric accuracy remains inferior to our method. This suggests that its region-partition-based structure preservation mechanism can improve the geometric fidelity of lightweight building models at the urban scale. However, the high diversity of building types and SLA's dependence on the quality of the initial region segmentation make it less robust in simplifying large-scale building models.

Table 5. Quantitative comparison of the proposed geometric structural constraint method with GH, LT, and SLA on large-scale urban building models under a compression ratio of 10%. RMSE and MAE are reported for evaluation.

Model	Initial Vertex #	Result Vertex #	RMSE (m)	MAE (m)	Method
SUM Part1	1,071,141	109,687	0.1131	0.0855	GH
			0.1650	0.1102	LT
			0.1413	0.1040	SLA
			0.0990	0.0754	Ours
SUM Part2	882,902	90,232	0.1125	0.0847	GH
			0.1705	0.1098	LT
			0.1033	0.1417	SLA
			0.0975	0.0738	Ours
STPLS3D USC	3,059,007	311,046	0.0786	0.0541	GH
			0.0853	0.0512	LT
			0.1344	0.0609	SLA
			0.0738	0.0449	Ours

The USC region of the STPLS3D dataset contains a large number of campus buildings with complex roof structures and irregular geometric details, which have higher requirements on the geometric feature preservation capability of simplification algorithms. In this region, the GH method achieves an RMSE of 0.0786 m and an MAE of 0.0541 m, while our geometry structural constrained method further reduces the RMSE to 0.0738 m and the MAE to 0.0449 m. In contrast, the LT method yields an RMSE of 0.0853 m and an MAE of 0.0512 m. The SLA method attains a higher RMSE of 0.1344 m and an MAE of 0.0609 m, indicating remarkably larger geometric errors than our method. This is attributed to the fact that our proposed geometric structural constraint assigns higher collapse costs to edges with high geometric saliency, which prioritizes edge collapse in geometrically flat and structurally regular regions. Our strategy effectively prevents the accumulation and propagation of errors over large-scale building surfaces and better preserves salient architectural geometric features, demonstrating its robustness in handling large building clusters with irregular and complex architectural structures.

The above experimental results validate the generalizability and robustness of the proposed geometry structural constrained method. When applied to large-scale urban models with irregular shapes, geometric discontinuities, and multi-scale structures, our method effectively reduces geometric errors induced and propagated in the edge collapse process.As a result, the overall geometric accuracy and structural fidelity of the simplified models are greatly improved compared with the GH, LT, and SLA methods. These findings complementarily verify the effectiveness of the proposed geometric structural constraint on the single-building experiments in Section 3.2. Furthermore, they provide a solid empirical foundation for subsequent experiments on our refined edge collapse method that incorporates dual constraints of geometric structure and building-component semantics.

3.4. Building Model Simplification Under Dual Constraints of Geometric Structure and Building Component Semantics

In the experiments of the previous sections, the collapse cost is mainly governed by local geometric saliency and normal inconsistency to prevent early edge collapses in highly salient regions and avoid the risk of face flipping. However, for building models with well-defined component-level structures, their key structural elements not only show salient geometric features but also exhibit explicit semantic boundaries. Semantic boundaries between building components, such as roofs and walls, or windows and window sills, are significant in preserving the interpretability and structural integrity of the building model. Collapsing edges across such semantic boundaries can lead to erroneous inter-part collapses, resulting in structural degeneration and local shape error propagation. Motivated

by this observation, we introduce semantic structural lines as an additional semantic constraint in the edge-collapse cost function, as detailed in Section 2.3. In our experiments, we chose five outdoor cultural heritage building scenes with relatively complete scans. Semantic point clouds of these scenes were converted into 3D mesh models via Poisson surface reconstruction [16]. We compared our refined edge-collapse under both geometric structural constraint and semantic constraint with the GH, LT, and SLA methods, under compression ratios of 30%, 10%, and 1%, respectively.

We reported the quantitative results in Table 6 and the 95% confidence intervals of RMSE and MAE in Table 7. For each model, the confidence intervals were estimated using bootstrap resampling over per-vertex errors with 1000 bootstrap resamples. Figure 15 presents the simplification results and error maps of our dual-constraint method at a 1% simplification ratio. As shown in Table 6, with the compression ratio progressively reducing from 30% to 1%, both RMSE and MAE increase due to the accumulation of edge-collapse errors. Our proposed structural–semantic dual-constraint simplification strategy achieves geometric accuracy comparable to that of the GH method at compression ratios of 30% and 10%, without introducing additional errors, and demonstrates stable error control under high compression ratios. Specifically, at ratios of 30% and 10%, the geometric errors of our method remain on par with the GH method, indicating that incorporating building component-level semantic constraints does not compromise the original edge-collapse framework. The semantic structural constraint regulates the collapse order by preventing early collapse of semantically important edges, while still allowing geometric error minimization. Therefore, the additional errors introduced by the semantic constraint are generally small, and their influence is compensated by the local quadratic error minimization to preserve the overall model geometry. When the compression ratio reaches 1%, the role of semantic boundaries in maintaining structural stability becomes a major factor determining the upper bound of the error. The advantage of the dual-constraint strategy is more clearly reflected in both the reduction in MAE and RMSE. Compared with the GH method, the RMSE of ArCH_1 decreases from 0.0237 m to 0.0234 m and the MAE from 0.0173 m to 0.0164 m. For ArCH_4, the RMSE decreases from 0.0098 m to 0.0095 m and the MAE from 0.0069 m to 0.0066 m. For ArCH_5, the RMSE is reduced from 0.0178 m to 0.0164 m, while the MAE decreases from 0.0131 m to 0.0118 m. Moreover, as shown in Table 6, under the 1% ratio, the LT and SLA methods yield significantly higher RMSE and MAE than the proposed dual-constraint method across all ArCH building models. This indicates that, for structurally complex cultural heritage buildings, simplification strategies that do not preserve architectural component-level structural constraints are more prone to inducing cross-component collapses and local structural degeneration, thereby further amplifying geometric errors.

It should be noted that for the ArCH_2 model at the ratio of 1%, our method shows an increase in RMSE while the MAE remains unchanged. This is due to the fact that RMSE is highly sensitive to the error distribution. If the mesh quality by projecting the semantic point cloud is limited, or if there exist inconsistencies between the regularized semantic structural lines and the original geometry, local geometric deviations may be introduced, resulting in an increased RMSE. In contrast, MAE, the average distribution of geometric errors over the entire model, remains stable. This indicates that the building component semantic constraint does not induce a significant degradation of geometric accuracy. Instead, the errors introduced are limited to a small number of localized regions and do not greatly affect the overall geometric fidelity of the model. In other words, the discrepancy between the semantic structural lines and the actual geometry yields an overall error level comparable to that obtained without semantic constraints. Moreover, the simplification results produced by our method exhibit more continuous component boundaries and more regularized local structures along semantic structural lines. Under high compression ratios, structural preservation has a higher priority

for maintaining the global geometry of architectural models. The contribution of semantic constraint is therefore not only reflected in reducing geometric errors, but rather in enhancing the stability of both structural integrity and semantic representation while keeping geometric accuracy within a reasonable range.

Table 6. Quantitative comparison of the proposed double-constrained method with GH, LT, and SLA on the ArCH cultural heritage building dataset under compression ratios of 30%, 10%, and 1%. RMSE and MAE are reported for evaluation.

Model	Compression Ratio 30%		Compression Ratio 10%		Compression Ratio 1%		Comparative Methods
	RMSE (m)	MAE (m)	RMSE (m)	MAE (m)	RMSE (m)	MAE (m)	
ArCH_1	0.0008	0.0006	0.0030	0.0022	0.0237	0.0173	GH
	0.0012	0.0008	0.0044	0.0030	0.0304	0.0202	LT
	0.0012	0.0008	0.0040	0.0029	0.0275	0.0195	SLA
	0.0009	0.0006	0.0032	0.0022	0.0234	0.0164	Ours
ArCH_2	0.0014	0.0011	0.0029	0.0022	0.0177	0.0132	GH
	0.0018	0.0014	0.0035	0.0025	0.0269	0.0158	LT
	0.0020	0.0015	0.0035	0.0026	0.0200	0.0146	SLA
	0.0013	0.0009	0.0033	0.0023	0.0186	0.0132	Ours
ArCH_3	0.0013	0.0009	0.0023	0.0018	0.0127	0.0092	GH
	0.0017	0.0012	0.0030	0.0021	0.0167	0.0117	LT
	0.0018	0.0013	0.0028	0.0021	0.0149	0.0110	SLA
	0.0008	0.0005	0.0023	0.0016	0.0133	0.0096	Ours
ArCH_4	0.0003	0.0002	0.0009	0.0006	0.0098	0.0069	GH
	0.0004	0.0003	0.0016	0.0011	0.0123	0.0081	LT
	0.0004	0.0003	0.0015	0.0010	0.0110	0.0079	SLA
	0.0006	0.0002	0.0010	0.0007	0.0095	0.0066	Ours
ArCH_5	0.0005	0.0003	0.0017	0.0012	0.0178	0.0131	GH
	0.0007	0.0004	0.0031	0.0020	0.0218	0.0147	LT
	0.0008	0.0004	0.0028	0.0019	0.0206	0.0151	SLA
	0.0005	0.0003	0.0018	0.0013	0.0165	0.0118	Ours

Table 7. Quantitative evaluation with 95% confidence intervals of RMSE and MAE for the proposed double-constrained method on the ArCH cultural heritage building dataset under a compression ratio of 1%. The confidence intervals were estimated using bootstrap resampling over per-vertex errors with 1000 bootstrap resamples.

Model	Initial Vertices #	Result Vertices #	Compression Ratio	RMSE (m)	95% CI	MAE (m)	95% CI
ArCH_1	105,547	1076	1%	0.0234	[0.0222, 0.0246]	0.0164	[0.0155, 0.0173]
ArCH_2	113,701	1159	1%	0.0186	[0.0176, 0.0197]	0.0132	[0.0126, 0.0138]
ArCH_3	273,066	2689	1%	0.0133	[0.0128, 0.0137]	0.0096	[0.0092, 0.0099]
ArCH_4	143,139	1456	1%	0.0095	[0.0091, 0.0099]	0.0066	[0.0062, 0.0069]
ArCH_5	143,706	1518	1%	0.0165	[0.0158, 0.0171]	0.0118	[0.0112, 0.0123]

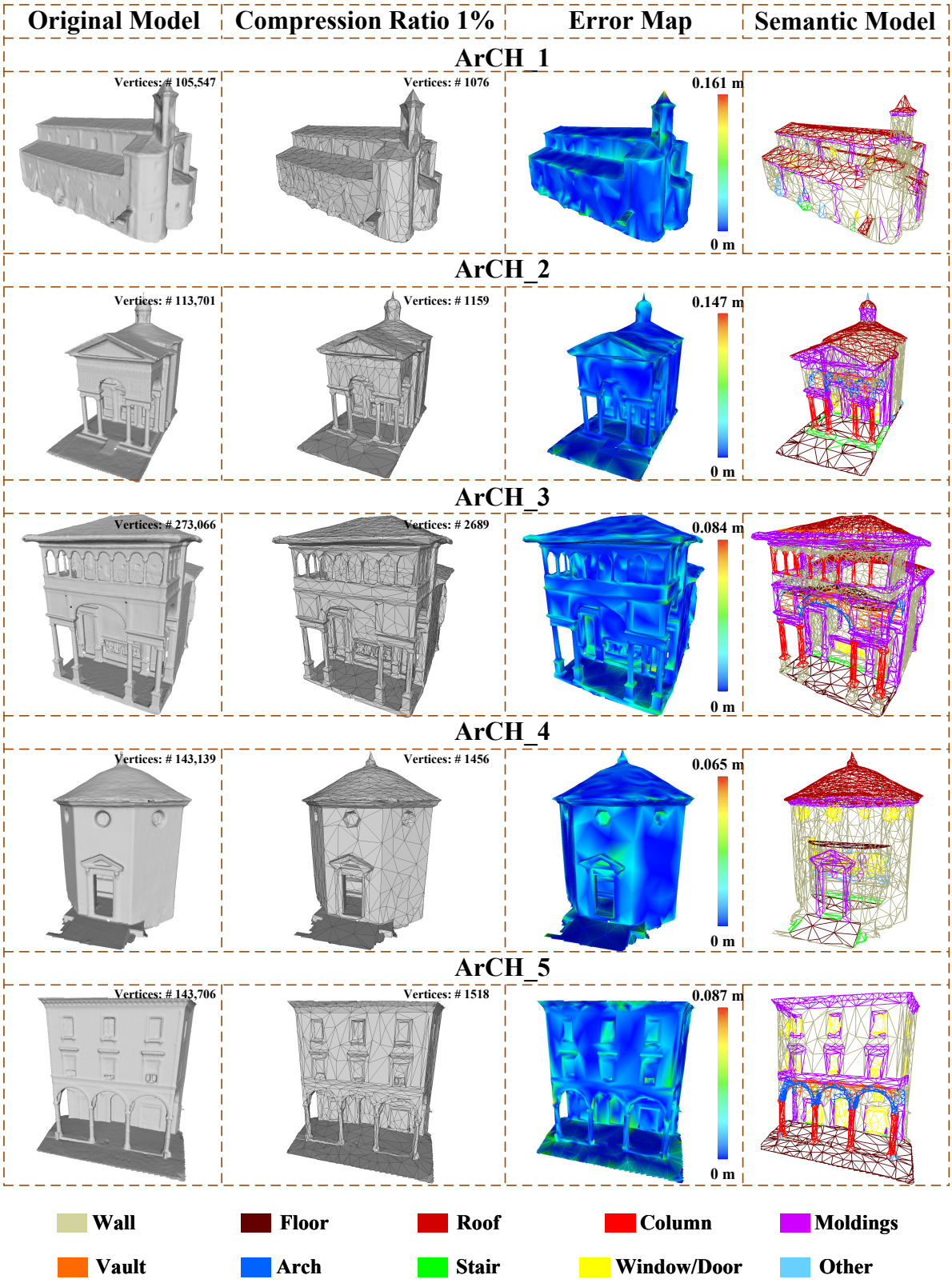

Figure 15. Simplification results of five cultural heritage buildings from the ArCH dataset using the proposed double-constrained method under a compression ratio of 1%. From left to right, the original model, the simplified model at 1% compression, the corresponding geometric error map, and the semantic models are presented.

Overall, Table 6 and Figure 15 demonstrate that the geometric-structure constraint is responsible for identifying and preserving local geometric features to reduce geometric er-

rors, while the building component semantic constraint further regulates the collapse order at component-level boundaries, preventing erroneous collapses across semantic regions and enabling the lightweight models to retain more reasonable architectural semantic structures. When both constraints are jointly imposed during model simplification, geometric accuracy is not degraded at simplification ratios of 30% and 10%. At a 1% simplification ratio, the combined constraints more effectively prevent error propagation due to structural collapse, generating simplified models that simultaneously achieve high geometric fidelity and enhanced structural interpretability. This provides reliable support for the subsequent construction of lightweight semantic models under the CityGML paradigm.

3.5. Ablation Studies

To further analyze the contribution of the building semantic constraint within the proposed edge-collapse framework, we performed ablation studies on the ArCH dataset comprising 5 models. The performance of the dual-constraint strategy was compared with variants using only geometric structural constraints, as well as the GH, LT, and SLA methods, under the same compression ratios. In this experiment, we aim to assess whether semantic structural lines can still provide additional benefits for error control when geometric saliency and normal inconsistency are already sufficient to prevent geometric degradation of building structures, especially at building component semantic boundaries.

As shown in Table 8, our proposed dual-constraint strategy consistently yields lower RMSE and MAE than the geometry-only structural constraint on most models. On ArCH_1, the dual-constraint approach achieves an RMSE of 0.0234 m and an MAE of 0.0164 m, while the geometry-only constraint achieves 0.0236 m and 0.0173 m, respectively. For ArCH_4, the dual-constraint errors are 0.0095 m and 0.0066 m, whereas the geometry-only constraint produces 0.0098 m and 0.0069 m. The greatest improvement is observed on ArCH_5, where the dual-constraint method achieves an RMSE of 0.0164 m and an MAE of 0.0118 m, in contrast to 0.0178 m and 0.0130 m under the geometry-only constraint. These results indicate that, even when geometric structural constraints already preserve major architectural structures, semantic constraints of building components can further reduce structural errors by preserving semantic boundary lines and mitigating erroneous cross-component merges. In addition, the geometric accuracy of the GH method demonstrates that an edge-collapse simplification strategy driven only by geometric error, without incorporating geometric feature awareness or semantic constraints, tends to collapse fine structural details at high compression ratios and lead to severe geometric deviations.

Table 8. Quantitative comparison of the proposed double-constrained method, the geometry-only constraint method, and GH, LT, and SLA on the ArCH cultural heritage building dataset under a compression ratio of 1%. RMSE and MAE are reported for evaluation.

Model	Geo. + Sem.(Ours)		Geometric Only		GH Method		LT Method		SLA Method	
	RMSE (m)	MAE (m)	RMSE (m)	MAE (m)	RMSE (m)	MAE (m)	RMSE (m)	MAE (m)	RMSE (m)	MAE (m)
ArCH_1	0.0234	0.0164	0.0236	0.0173	0.0237	0.0173	0.0304	0.0202	0.0275	0.0195
ArCH_2	0.0186	0.0132	0.0186	0.0132	0.0177	0.0132	0.0269	0.0158	0.0200	0.0146
ArCH_3	0.0133	0.0096	0.0126	0.0092	0.0127	0.0092	0.0167	0.0117	0.0149	0.0110
ArCH_4	0.0095	0.0066	0.0098	0.0069	0.0098	0.0069	0.0123	0.0081	0.0110	0.0079
ArCH_5	0.0164	0.0118	0.0178	0.0130	0.0178	0.0131	0.0218	0.0147	0.0206	0.0151

Table 8 also shows that for the ArCH_2 and ArCH_3 models, the errors under the dual-constraint setting are on-par or slightly higher than the geometry-only structural constraint.

This indicates that the effectiveness of semantic constraints on building components is related to the quality of the semantic input, as well as the consistency between semantic boundaries and mesh geometry. When the extracted semantic structural lines contain noise or shape deviations induced by the optimization and regularization, the semantic constraint term may lead to a degradation of local geometric accuracy with increased RMSE and MAE values. Nevertheless, the resultant RMSE and MAE are comparable with the values obtained by the geometry-only constraint strategy, demonstrating that our dual-constraint method is robust even in the presence of errors in semantic structural line extraction. These observations also point to a clear direction for further improvement. Specifically, we can enhance the consistency between semantic structural lines and building geometry by using more robust semantic projection strategies, so as to encourage the semantic constraint to provide stable performance gains.

From both Tables 6 and 8, it can be seen that built upon the geometric constraint guided by geometric saliency and normal inconsistency, semantic constraints of building components can further refine the edge-collapse sequence along semantic structural boundaries. At a compression ratio of 1%, incorporating semantic constraints effectively reduces cross-semantic-region collapses and avoids structural degradation of building models. The simplified results consistently exhibit higher geometric accuracy than those produced by the GH, LT, and SLA methods.

3.6. Comparison Experiments

(1) Comparison with recent general mesh simplification methods

To evaluate the performance of the proposed dual-constraint simplification framework against recent advances in general 3D mesh simplification, we conducted comparative experiments on the ArCH dataset. Our method was compared with two recent state-of-the-art approaches, Robust Low-Poly Meshing for General 3D Models (RoLoPM) [55] and Parallel Mesh Optimization for Intersection-Free Low-Poly Modeling on the GPU (PaMO) [56]. The ArCH dataset contains detailed architectural meshes with complex geometric structures and provides a representative benchmark for evaluating the geometric fidelity of simplified building models.

RoLoPM reconstructs a clean proxy mesh from the unsigned distance field of the input model, iteratively performing edge-collapse simplification combined with geometric flow and normal-based feature alignment to preserve sharp features and geometric appearance. PaMO proposes a GPU-based mesh optimization framework that performs remeshing using distance fields and Dual Marching Cubes, followed by parallel edge-collapse simplification and collision-aware safe projection to efficiently generate intersection-free low-poly meshes.

The quantitative results in Table 9 show that our method consistently achieves lower RMSE and MAE values across all tested models compared with RoLoPM and PaMO, indicating better geometric fidelity after simplification. Figure 16 further illustrates the visual comparison using the representative model ArCH_2. As highlighted in the enlarged regions, our method better preserves architectural fine details. In comparison, PaMO oversimplifies structural regions, leading to noticeable structural collapse of the mesh models. This is mainly because PaMO focuses on parallel mesh optimization and intersection-free simplification without explicitly modeling architectural structural constraints. RoLoPM partially recovers geometric features through geometric flow and normal-based feature alignment. However, its feature preservation remains limited since the method primarily targets general 3D models and does not incorporate explicit structural constraints for architectural components.

Table 9. Quantitative comparison of the proposed method with RoLoPM and PaMO on the ArCH cultural heritage building dataset under a compression ratio of 1%. RMSE and MAE are reported for evaluation.

Model	Compression Ratio	RMSE (m)	MAE (m)	Comparative Methods
ArCH_1	1%	0.0395	0.0282	RoLoPM
		0.0385	0.0308	PaMO
		0.0234	0.0164	Ours
ArCH_2	1%	0.0314	0.0219	RoLoPM
		0.0283	0.0230	PaMO
		0.0186	0.0132	Ours
ArCH_3	1%	0.0148	0.0098	RoLoPM
		0.0297	0.0245	PaMO
		0.0133	0.0096	Ours
ArCH_4	1%	0.0163	0.0120	RoLoPM
		0.0164	0.0131	PaMO
		0.0095	0.0066	Ours
ArCH_5	1%	0.0247	0.0171	RoLoPM
		0.0340	0.0278	PaMO
		0.0165	0.0118	Ours

Benefiting from the joint geometric-structural and semantic constraints embedded in the edge-collapse cost function, our method can better preserve critical architectural structures during simplification while maintaining overall geometric accuracy.

(2) Comparison with structure-preserving building simplification methods

To analyze the performance of different structure-preservation strategies in real-world, large-scale urban scenes, we conducted comparative experiments on the Graz urban building dataset. Our proposed method was evaluated against two representative approaches introduced in the past five years, the feature-preserving method [14] and the shape-preserving method [15]. For completeness, we also report the results of two recent general mesh simplification approaches, RoLoPM [55] and PaMO [56], under the same experimental setting. The Graz urban building mesh has a length of approximately 890m and a width of 350 m, comprising 1.6 million vertices and 3.1 million faces. The feature-preserving method models building geometry as regular planar structures. It adopts bilateral filtering to enhance planar features and extracts planar regions such as roofs and facades through region growing to preserve planar regularity during simplification. The shape-preserving method embeds the gradient structure tensor as a structural constraint into the edge-collapse simplification. Different weights are assigned to linear primitives, nonlinear primitives, and structural lines, which further increases the collapse cost of key features such as roof ridges, block edges, and facade contours.

Compared with the feature-preserving method and the shape-preserving method, our method differs in two aspects. First, instead of using planar assumptions, we directly identify key structural regions through joint geometric structural and semantic constraints, preserving key structural details without explicit planar segmentation. Second, unlike the shape-preserving method that relies purely on geometric constraints, our method further incorporates semantic constraints by detecting semantic structural boundaries across components and embedding them into the edge-collapse cost function. This mutually enhances both structural stability and semantic expressiveness of the simplified model. For comparison, we set the same compression ratio of 3% for all methods. The geometric errors and visual simplification results are reported in Table 10 and Figure 17.

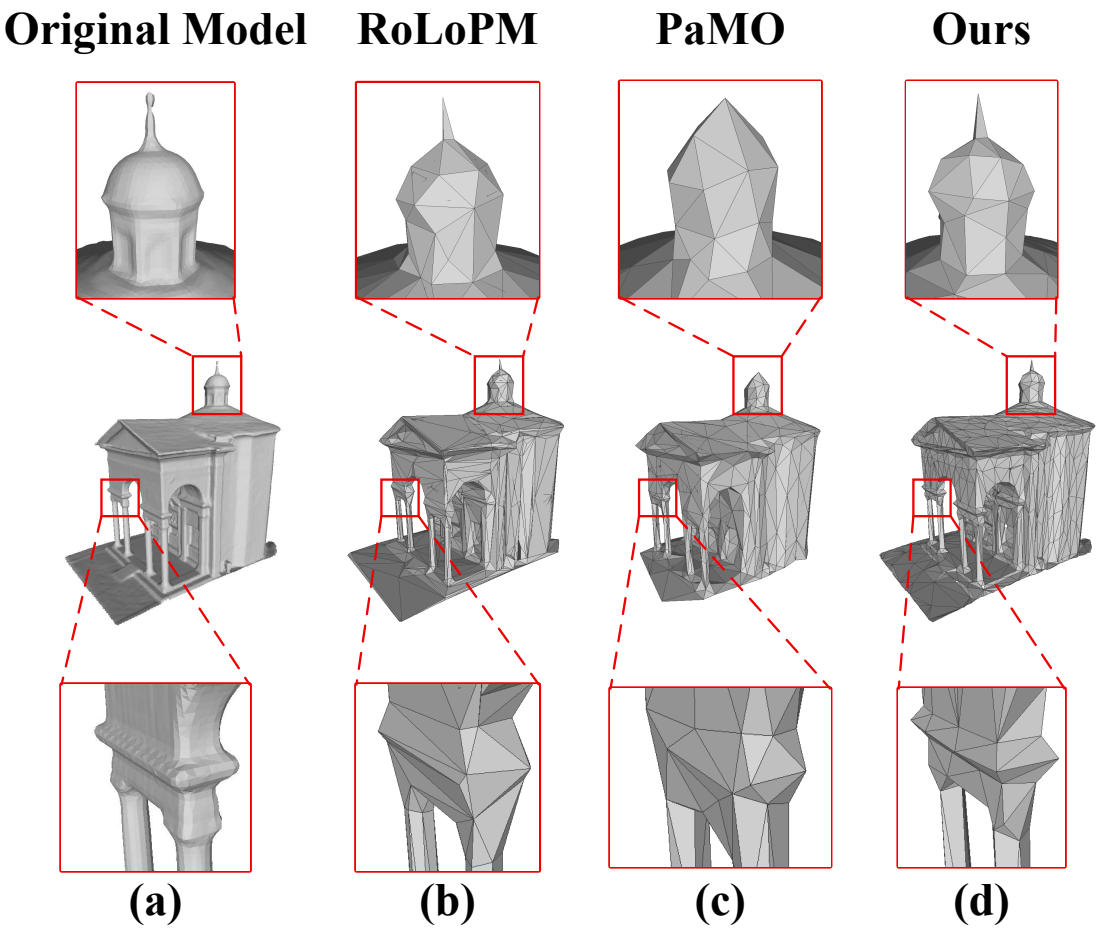

Figure 16. Visual comparison of structural detail preservation among RoLoPM, PaMO, and the proposed method under a compression ratio of 1% on the ArCH_2 model from the ArCH dataset. Subfigures (**a**–**d**) show the original model, the simplification results produced by RoLoPM, PaMO, and the proposed method, respectively. The red boxes indicate representative structural regions and their enlarged views for detailed comparison.

As shown in Table 10, under the same compression rate of 3%, our method achieves higher geometric accuracy on the Graz dataset than the feature-preserving method, attaining an RMSE of 0.65 m and an MAE of 0.38 m, which are respectively 0.10 m and 0.06 m lower than the feature-preserving method. These results indicate that, in complex real-world urban-scale building scenes, a strategy that regulates the edge-collapse based on geometric structural constraints yields more stable improvements on global geometric accuracy. In comparison, the feature-preserving method is based on the geometric assumption that buildings are mainly composed of piecewise planar surfaces. However, in large-scale urban scenes such as Graz, building models often contain a large number of small-scale complex structures that are non-planar or weakly planar, such as chimneys, skylights, and roof-mounted attachments. Under the planar assumption, these structures tend to be treated as noise or secondary geometric components. Therefore, this method shows larger RMSE and MAE values on the Graz dataset due to the loss of these fine geometric details. Similarly, the two general mesh simplification methods, RoLoPM and PaMO, exhibit significantly larger RMSE and MAE values on the Graz dataset. This is mainly because these approaches are designed for general 3D models and do not explicitly incorporate architectural structural constraints, which makes them less effective in preserving structural details in large-scale urban building scenes.

Table 10. Quantitative comparison of the proposed method with feature-preserving, shape-preserving, RoLoPM, and PaMO methods on the Graz dataset.

Comparative Methods	Compression Ratio	RMSE (m)	MAE (m)
Feature-preserving Method [14]	3%	0.75	0.44
Shape-preserving Method [15]	3%	0.27	0.38
RoLoPM [55]	3%	2.76	2.09
PaMO [56]	3%	2.21	2.02
Ours	3%	0.65	0.38

Unlike the feature-preserving method, our method does not rely on planar assumptions. It directly optimizes the edge-collapse sequence according to geometric saliency and normal inconsistency. Vertices with higher geometric saliency are assigned higher preservation priority to better maintain local, non-planar structural details such as chimneys and skylights, leading to lower geometric errors on the Graz dataset and thus demonstrating stronger capability in complex urban scenes.

Compared with the shape-preserving method, our method yields a slightly higher RMSE due to a few localized outliers, while both methods achieve the same MAE of 0.38 m. This result indicates that the two methods show comparable behavior in the mean distribution of overall geometric error. The observed difference in RMSE is mainly attributed to large geometric deviations in a limited number of local regions. The shape-preserving method incorporates the semantics of linear and nonlinear geometric primitives, introducing them as constraints to enforce the simplified model to conform as closely as possible to the global shape skeleton. As a result, it retains critical geometric details and achieves the lowest geometric error on the Graz dataset.

In contrast, our method characterizes structural importance purely from the perspectives of geometric saliency and normal inconsistency, without further distinguishing the hierarchical roles of different types of geometric features. Under extreme compression conditions, this may still lead to larger shape deviations at a small number of key structural locations, resulting in a higher RMSE compared to the shape-preserving method.

3.7. Lightweight Building Semantic Representation Under CityGML Paradigm

Building semantic modelling aims to achieve a consistent representation of building entity attributes and inter-entity relationships through a standardized paradigm, which allows the model to be recognized, interpreted, and exploited by computers for subsequent analytical tasks. To enhance the computability and applicability of the model so as to better support downstream scientific applications, our method preserves and inherits the semantic information of building components from the original semantic point cloud, and stores this information under the standardized CityGML paradigm. CityGML represents an international standard for 3D urban modelling established by the Open Geospatial Consortium (OGC). Its core principle is integrating representations of building geometry, semantic structures, and hierarchical relationships among these structures together. By explicitly modelling building objects, component types, and their spatial relationships, 3D building models can simultaneously support geometric visualization, semantic querying, and application-oriented analysis.

This study further incorporates the lightweight building semantic models obtained from Section 3.4 into the CityGML paradigm. Five building models from the ArCH dataset were selected and generated using the proposed dual-constraint edge-collapse that jointly considers geometric structure and building-component semantic structure, under a compression ratio of 1%. These models contain rich building component semantic

information and include nine types of architectural elements, such as roofs, walls, doors and windows, columns, and arches. Semantic reorganization and hierarchical mapping are performed for the five lightweight building semantic models under the CityGML 2.0 standard, targeting LoD3 with detailed building facade components. The visualization results are shown in Figure 18. The architectural heritage component semantics provided by the ArCH dataset are organized into the predefined BoundarySurface system of CityGML. Taking the ArCH_2 building model as an example, its corresponding data structure and semantic class mapping are illustrated in Figure 19. Furthermore, the generated models exhibit structural validity and compliance with the CityGML standard, and can be imported into KITModelViewer (https://www.iai.kit.edu/IAI-Energiesystemanalyse.php, accessed on 14 March 2026) for semantic parsing and visualization (Figure 20).

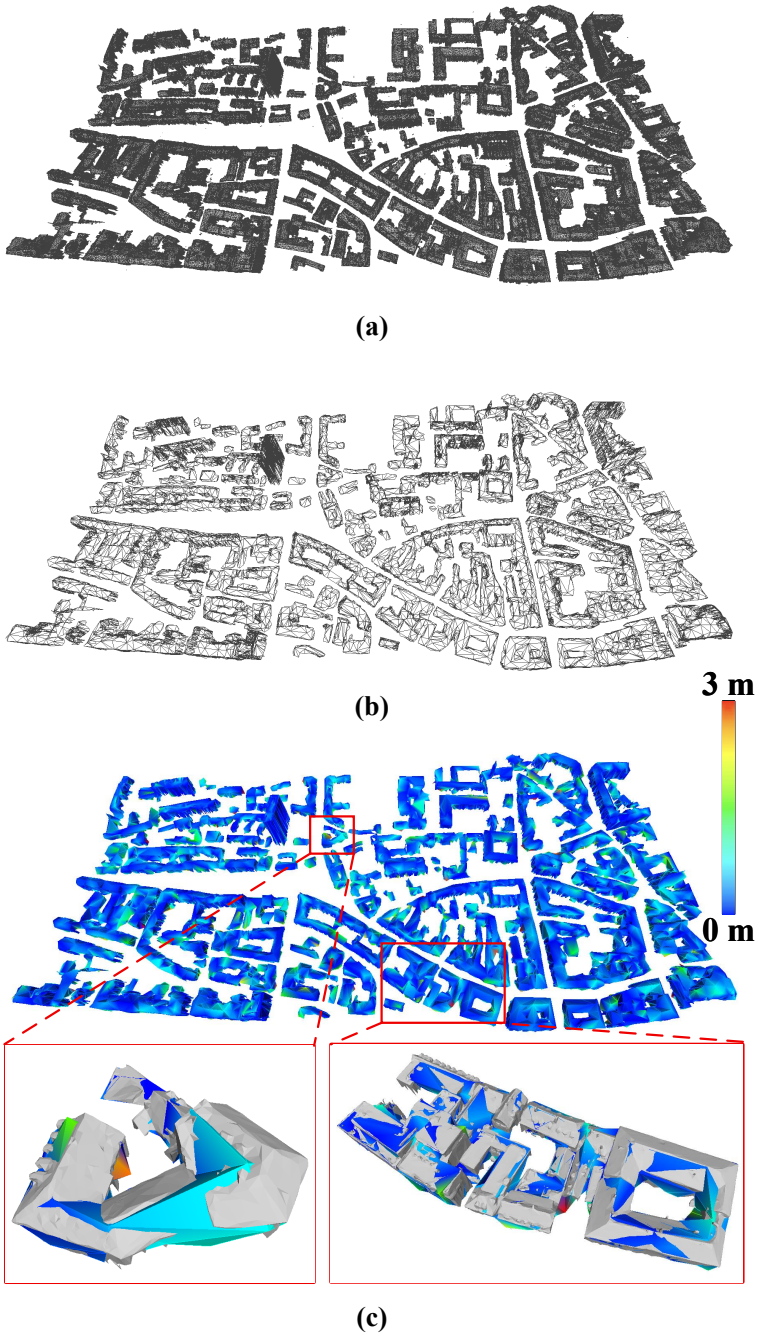

Figure 17. Simplification results of the Graz urban building mesh model using the proposed method under a compression ratio of 3%. Subfigure (**a**) presents the original Graz mesh model, (**b**) shows the simplification result at 3% compression, and (**c**) displays the corresponding geometric error map.

Under the CityGML paradigm, we achieve an effective integration of lightweight geometric building models with cultural heritage component semantics. The generated models simultaneously exhibit geometric compactness, semantic richness, and compliance to CityGML standard, providing stable and reliable data support for downstream semantic querying, architectural component analysis, and other applications.

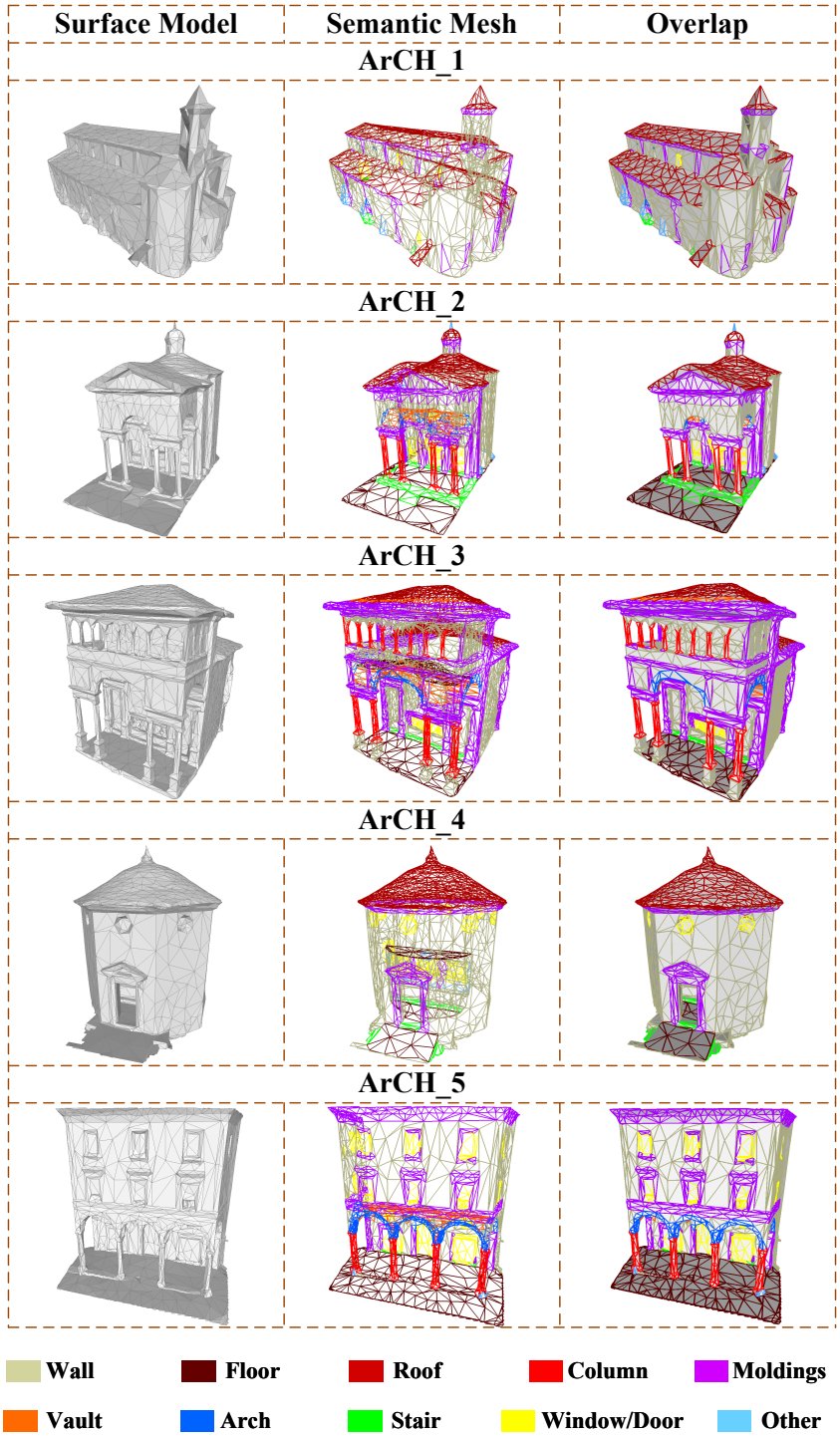

Figure 18. Lightweight semantic building mesh models generated by the proposed double-constrained method under a compression ratio of 1% on the ArCH dataset. From left to right, the surface-filled model, the semantic building mesh model, and their overlaid visualization are presented.

```
<core:CityModel xmlns:bldg="http://www.opengis.net/citygml/building/2.0" xmlns:core="http://www.opengis.net/citygml/2.0">
  <gml:boundedBy>
  <core:cityObjectMember>
    <bldg:Building gml:id="5_SMV_chapel_1">
      <gml:name>5_SMV_chapel_1</gml:name>
      <bldg:boundedBy>                                                    ..... WallSurface
        <bldg:WallSurface gml:id="WallSurface_wallSurface">
          <gml:name>sem:wallSurface</gml:name>
          <bldg:_GenericApplicationPropertyOfBoundarySurface>           ..... wall
          <bldg:lod3MultiSurface>
        </bldg:WallSurface>
      </bldg:boundedBy>
      <bldg:boundedBy>
        <bldg:WallSurface gml:id="WallSurface_windows_door">
          <gml:name>sem:windows_doorSurface</gml:name>
          <bldg:_GenericApplicationPropertyOfBoundarySurface>           ..... window/door
          <bldg:lod3MultiSurface>
        </bldg:WallSurface>
      </bldg:boundedBy>
      <bldg:boundedBy>
        <bldg:WallSurface gml:id="WallSurface_moldingsSurface">
          <gml:name>sem:moldingsSurface</gml:name>
          <bldg:_GenericApplicationPropertyOfBoundarySurface>           ..... moldings
          <bldg:lod3MultiSurface>
        </bldg:WallSurface>
      </bldg:boundedBy>

      <bldg:boundedBy>                                                    ..... RoofSurface
        <bldg:RoofSurface gml:id="RoofSurface_roofSurface">             ..... roof
      </bldg:boundedBy>

      <bldg:boundedBy>                                                    ..... FloorSurface
        <bldg:FloorSurface gml:id="FloorSurface_floorSurface">          ..... floor
      </bldg:boundedBy>

      <bldg:boundedBy>                                                    ..... CeilingSurface
        <bldg:CeilingSurface gml:id="CeilingSurface_vaultSurface">      ..... vault
      </bldg:boundedBy>
      <bldg:boundedBy>
        <bldg:CeilingSurface gml:id="CeilingSurface_archSurface">       ..... arch
      </bldg:boundedBy>

      <bldg:outerBuildingInstallation>                                    ..... BuildingInstallation
        <bldg:BuildingInstallation gml:id="columnSurface">              ..... column
      </bldg:outerBuildingInstallation>
      <bldg:outerBuildingInstallation>
        <bldg:BuildingInstallation gml:id="stairSurface">               ..... stair
      </bldg:outerBuildingInstallation>
      <bldg:outerBuildingInstallation>
        <bldg:BuildingInstallation gml:id="otherSurface">               ..... other
      </bldg:outerBuildingInstallation>
    </bldg:Building>
  </core:cityObjectMember>
</core:CityModel>
```

Figure 19. Data structure of the lightweight semantic building model of ArCH_2 under the CityGML paradigm (geometric information omitted for clarity).

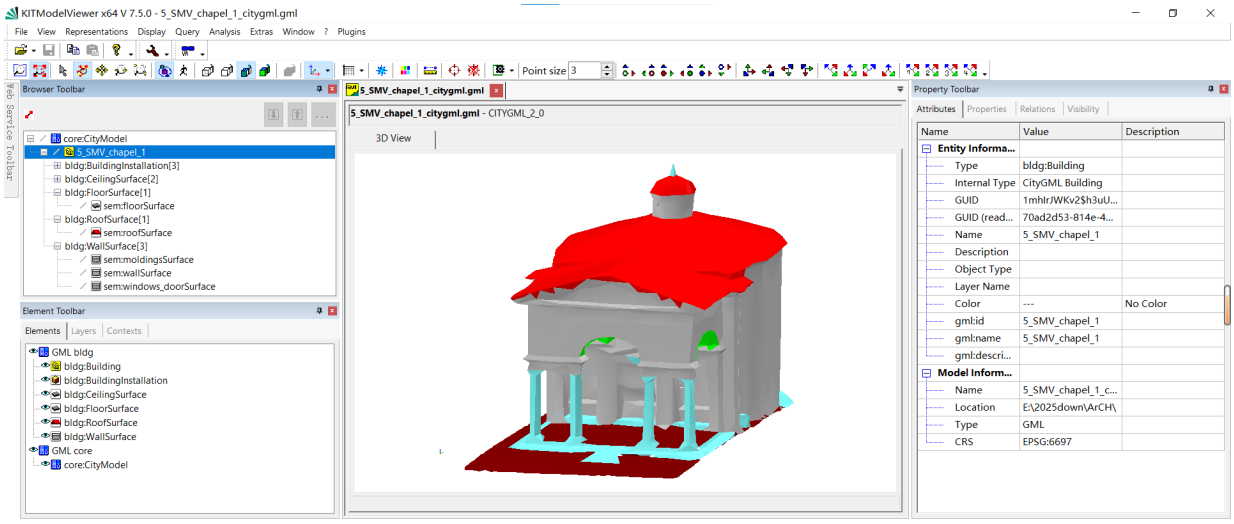

Figure 20. Lightweight semantic building model of ArCH_2 under the CityGML paradigm, visualized in KITModelViewer at a compression ratio of 1%.

4. Discussion

We have extensively evaluated the proposed dual-constrained simplification method on multiple datasets of varying scales, geometries, and complexities, including the 40 single-building models from Sketchlab, the city-scale urban building cluster datasets SUM, STPLS3D, and Graz, as well as the cultural heritage dataset ArCH. Overall, the experimental results clearly demonstrate that our proposed dual-constrained method has achieved superior or comparable performance compared to all the existing methods by consistently reducing the geometric errors of the simplified models. Specifically, the geometric structural constraints based on geometric saliency and local normal inconsistency effectively improve the geometric accuracy of model simplification on both the single-building models and city-scale building cluster datasets. Enhanced with building semantic constraints, our method further prevents structural degradation due to cross-component collapses, achieving better or on-par performance on the cultural heritage dataset and the Graz urban-scale building dataset. We also standardize the semantic representation and storage of lightweight building models under the CityGML paradigm, which provides a unified data support for downstream sharing, analysis, and applications of building models.

In subsequent sections, we provide a comprehensive analysis of the sensitivity of important parameters used in our method, as well as the limitations and potential future research directions.

4.1. Parameter Sensitivity Analysis

To validate the rationality of the parameter settings used in the experiments, we performed a sensitivity analysis on three key parameters affecting the edge-collapse optimization process, including the geometric saliency threshold T_g, the normal inconsistency threshold T_α, and the weight coefficient of the geometric structural constraint w. Two models, ArCH_1 and ArCH_5, from the ArCH dataset were chosen for this analysis. We set the compression ratio as 1%, and evaluated the simplification errors of different parameter settings under the metrics of RMSE and MAE.

(1) Sensitivity analysis of the geometric saliency threshold T_g.

T_g is used to identify geometrically salient regions in the building model. Edges that have vertices with saliency values higher than this threshold are assigned higher collapse costs to preserve key geometric structures. We varied T_g from 0.05 to 0.90 while keeping other parameters fixed, recording the corresponding errors in Figure 21. As T_g increases, both RMSE and MAE change smoothly, indicating its limited influence on overall geometric error. Experimental results show that when $T_g < 0.6$, too many edges are identified as salient, which weakens the discriminative capability of this constraint. When $T_g > 0.75$, a number of salient edges cannot be preserved, degrading the fine-structural details. An T_g between 0.6 and 0.75 leads to small and stable geometric errors. Therefore, we recommend $T_g = 0.65$ in our experiments.

(2) Sensitivity analysis of the normal inconsistency threshold T_α.

T_α is used to detect abrupt local normal variations or potential surface triangle folding in the mesh model. When the maximum angular deviation between the vertex normal and the face normals in the first-ring neighborhood of this vertex exceeds T_α, the associated edges are assigned more penalty costs during the edge collapse. We changed the value of T_α from 30° to 180° while keeping the other parameters fixed. The corresponding RMSE and MAE values were recorded, as shown in Figure 22. As T_α increases from 30° to 60°, the RMSE of both models decreases. When it exceeds 60°, RMSE and MAE remain nearly stable, indicating that the influence of T_α becomes limited. Therefore, T_a is set as 60° in this study to ensure stable simplification results.

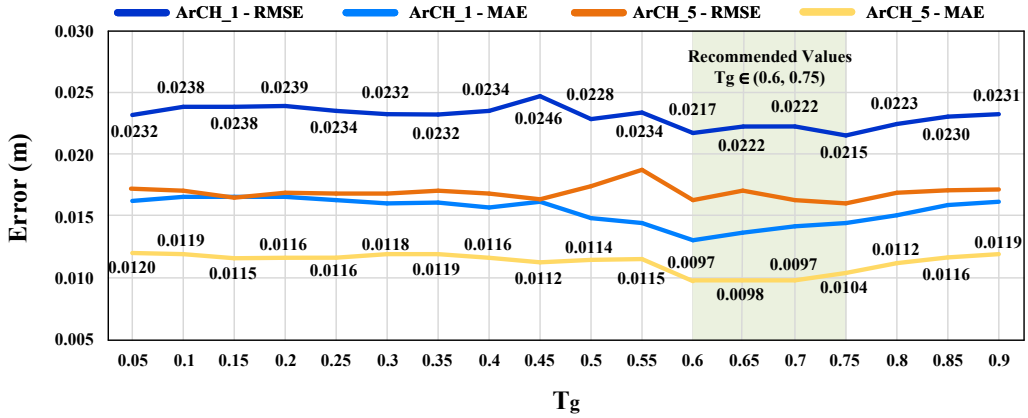

Figure 21. Sensitivity analysis of the geometric saliency threshold T_g. RMSE and MAE of the simplified models are evaluated under different T_g values using ArCH_1 and ArCH_5 at a compression ratio of 1%. The shaded region indicates the recommended parameter range.

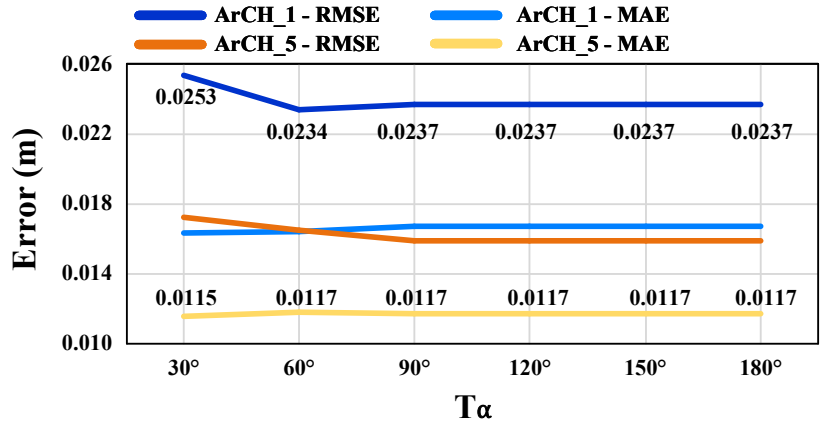

Figure 22. Sensitivity analysis of the normal inconsistency threshold T_α. RMSE and MAE obtained on ArCH_1 and ArCH_5 are plotted for different T_α values under a compression ratio of 1%.

(3) Sensitivity analysis of the weight w.

In our method, structural edges participate in the edge-collapse cost through an exponential penalty mechanism (see Equation (18)). When a candidate edge satisfies multiple constraints, its collapse cost is amplified by w^N, with N being the number of satisfied constraints. This delays the collapse of edges that represent critical geometric or semantic structures to preserve key building features. In this experiment, we varied w from 5 to 25 while keeping the other parameters fixed. The corresponding RMSE and MAE values are shown in Figure 23. As w increases, both RMSE and MAE vary smoothly without noticeable fluctuations. When $w = 10$, the errors begin to stabilize. Further increases of w lead to only minor performance changes, indicating that the weight does not significantly affect the overall geometric accuracy of the simplified model when penalizing edges that satisfy multiple constraints. Therefore, $w = 10$ is adopted as the default value in this study.

4.2. Limitations and Future Work

Although our proposed dual-constrained building mesh simplification method has demonstrated its effectiveness and robustness across multi datasets in complex urban environments, it still suffers from several limitations.

First, our method mainly mitigates structural degradation by regulating the edge collapse sequence. However, a few resultant models still exhibit insufficient geometric regularity (e.g., edge straightness and surface planarity). How to enhance the model

geometric regularity remains an open research question. For building components with curved surfaces and nonlinear structural elements, we may explore hybrid representations by integrating parametric modelling with mesh simplification to improve the representation fidelity of complex-shaped buildings while maintaining model lightweightness.

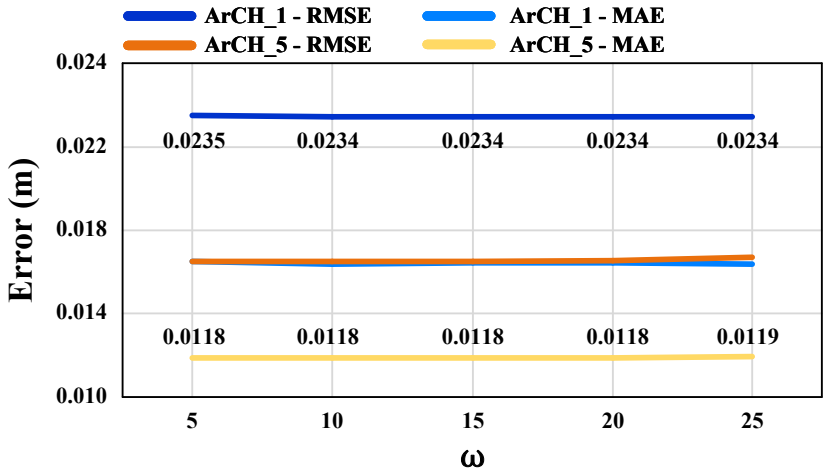

Figure 23. Sensitivity analysis of the weight coefficient w in the structural constraint term. RMSE and MAE of the simplified models are reported for different values of w on ArCH_1 and ArCH_5 under a compression ratio of 1%.

In addition, this study mainly focuses on the representation and preservation of geometric structures and component-level semantic structure, without considering texture information. Future work will incorporate texture atlases to construct semantic mesh models with texture attributes, enhancing the lightweight semantic building models with more realistic texture-semantic representations to extend their applicability for downstream tasks such as photorealistic rendering and digital cultural heritage visualization.

Furthermore, our method assumes that the input point clouds and mesh models are structurally complete. In practice, the performance of the proposed constraints is influenced by the quality of the input data. The geometric structural constraints rely on the completeness of the reconstructed geometry, which depends on the integrity of the input point clouds and the adopted 3D reconstruction method. If the reconstructed geometry contains missing structures or inaccuracies, the detected geometric features may also be incomplete. Meanwhile, the semantic structural constraints depend on the reliability and granularity of the semantic labels. Semantic noise caused by annotation or recognition errors may introduce short irregular branches in the semantic structural lines. To alleviate this issue, our method partially mitigates such noise by removing short connected branches in the semantic structural lines. In addition, if the semantic annotations only provide coarse primitive-level labels (e.g., wall or roof surfaces) rather than component-level labels (e.g., doors or windows), the proposed semantic constraints cannot explicitly preserve the boundaries of these fine-scale components. To address this issue, we will incorporate data completion and repair procedures in our method. Specifically, the completeness of point clouds can be improved by oversampling-based completion models such as APC2Mesh, while incomplete mesh models with defects such as holes can be preprocessed using mesh-editing tools (e.g., CloudCompare) to mitigate the geometric distortions, which reduces their impact on simplification results. Similarly, the semantic quality of the input point clouds can be improved through semantic denoising or hierarchical semantic refinement strategies, which would enable the semantic constraints to more effectively preserve the structural characteristics of building components.

5. Conclusions

To address the problems of geometric structure degradation and inconsistency of building-component semantics in building model simplification under high compression ratios, this study proposes a structural–semantic dual-constrained edge-collapse method. Built upon the classical QEM approach, geometric saliency, normal inconsistency, and building-component semantics are incorporated as constraints to jointly preserve building geometric accuracy and structural interpretability. Compared with conventional methods that aim purely at minimizing geometric error, our method optimizes the edge-collapse sequence based on both geometric and semantic significance, assigning higher preservation priority to regions with key geometric and semantic structures.

Experimental results on datasets of different scales and complexities demonstrate that our method consistently achieves superior geometric accuracy across single-building models, city-scale building clusters, and cultural heritage models with building component semantics. On individual building models from Sketchfab, we have achieved lower RMSE and MAE than the GH, LT, and SLA methods under the same compression ratios, indicating that regulating the collapse sequence based on geometric saliency and normal inconsistency effectively prevents error accumulation due to local shape deviations and detail degradation. On the city-scale building dataset Graz, our proposed method reduces RMSE and MAE by 13.3% and 13.6%, respectively, relative to the feature-preserving method, and achieves comparable performance to the shape-preserving method in terms of MAE. Furthermore, on the large-scale SUM and STPLS3D urban datasets, our method reduces RMSE by approximately 6.1–13.3% and MAE by approximately 11.8–17.0% compared with the GH method. All these results demonstrate the strong robustness and generalizability of our method against complex architectural morphologies and large-scale urban structures. Experiments on the ArCH cultural heritage building dataset further demonstrate that, under extreme compression ratios, pure geometric constraints are insufficient to prevent structural degradation due to cross-component edge collapses. Incorporating semantic constraints can effectively regulate the collapse sequence at component semantic boundaries to avoid structural collapse and semantic inconsistency. Under a compression ratio of 1%, the proposed dual-constrained method generates lightweight building models with lower reconstruction errors compared with the GH method, with the RMSE reduced by 7.3% and the MAE reduced by 9.9%. In this dual-constraint method, geometric structural constraints and building component semantic constraints jointly guide the optimization of the edge-collapse sequence. The former focus on preserving local geometric features, while the latter regulates collapse operations at critical structural regions. Integrating both constraints jointly enables accurate geometric representation and structural fidelity even under high compression ratios.

We aim to further improve the practicality of our method by developing application-oriented and customized simplification strategies tailored for specific use cases. For different applications, such as building simulation, digital archiving, cultural heritage restoration, and extended reality (XR) visualization, we can incorporate task-relevant criteria to construct an application-driven building model simplification framework. This will enhance the adaptability and practical value of lightweight semantic building models on diverse scenarios and tasks.

Author Contributions: C.Z. and D.C. analyzed the data and wrote source code. S.D. and Z.C. helped in project and study design, paper writing, and data analysis. Y.W. assisted in supervision, funding acquisition, and conceptualization. M.S. helped in proofreading, data acquisition, and experiment comparison. Y.K. and S.F. assisted in figure and table preparation. J.P. and L.Z. provided constructive comments and assisted in proofreading. All authors have read and agreed to the published version of the manuscript.

Funding: This work was supported in part by the National Natural Science Foundation of China under Grant 42271450, in part by the Major Program of the National Natural Science Foundation of China under Grant 42293272, in part by the Open Fund of Key Laboratory of Urban Land Resources Monitoring and Simulation, Ministry of Natural Resources under Grant KF-2023-08-15, and in part by the Project of Practical Training for Science and Engineering Teachers from Colleges and Universities in Anhui Province in Enterprises under Grant 2024jsqygz109.

Data Availability Statement: The datasets used in this study are available from their respective sources. The Sketchfab building models can be accessed at https://sketchfab.com/, accessed on 14 March 2026. The SUM dataset is available at https://3d.bk.tudelft.nl/projects/meshannotation/, accessed on 14 March 2026. The STPLS3D dataset is available at https://www.stpls3d.com/, accessed on 14 March 2026. The ArCH dataset is available at https://archdataset.polito.it/, accessed on 14 March 2026. The Graz dataset was kindly provided by Dr. Minglei Li from Nanjing University of Aeronautics and Astronautics.

Conflicts of Interest: The authors declare no conflicts of interest.

References

1. Biljecki, F.; Stoter, J.; Ledoux, H.; Zlatanova, S.; Çöltekin, A. Applications of 3D city models: State of the art review. *ISPRS Int. J.-Geo-Inf.* **2015**, *4*, 2842–2889. [CrossRef]
2. Kolbe, T.H.; Donaubauer, A. Semantic 3D city modeling and BIM. In *Urban Informatics*; Springer: Berlin/Heidelberg, Germany, 2021; pp. 609–636.
3. Bieringer, A.; Wysocki, O.; Tuttas, S.; Hoegner, L.; Holst, C. Analyzing The Impact Of Semantic Lod3 Building Models On Image-Based Vehicle Localization. *ISPRS Ann. Photogramm. Remote Sens. Spat. Inf. Sci.* **2024**, *4*, 55–62. [CrossRef]
4. Xie, H.; Chen, Z.; Hong, F.; Liu, Z. Citydreamer: Compositional generative model of unbounded 3d cities. In *Proceedings of the IEEE/CVF Conference on Computer Vision and Pattern Recognition*; IEEE: Piscataway, NJ, USA, 2024; pp. 9666–9675.
5. Chen, S.; Miranda, F.; Ferreira, N.; Lage, M.; Doraiswamy, H.; Brenner, C.; Defanti, C.; Koutsoubis, M.; Wilson, L.; Perlin, K.; et al. UrbanRama: Navigating cities in virtual reality. *IEEE Trans. Vis. Comput. Graph.* **2021**, *28*, 4685–4699. [CrossRef]
6. Chen, D.; Zhu, C.; Zhang, Z.; Na, J.; Shen, Y.; Chen, Y.; Peethambaran, J.; Zhang, L. Public Building Geometric Models From Point Clouds: A multidimensional quality evaluation framework. *IEEE Geosci. Remote Sens. Mag.* **2025**, *14*, 335–361. [CrossRef]
7. Zhang, K.; Yan, J.; Chen, S.C. Automatic construction of building footprints from airborne LIDAR data. *IEEE Trans. Geosci. Remote Sens.* **2006**, *44*, 2523–2533. [CrossRef]
8. Du, S.; Zhang, Y.; Zou, Z.; Xu, S.; He, X.; Chen, S. Automatic building extraction from LiDAR data fusion of point and grid-based features. *ISPRS J. Photogramm. Remote Sens.* **2017**, *130*, 294–307. [CrossRef]
9. Verma, V.; Kumar, R.; Hsu, S. 3D building detection and modeling from aerial LIDAR data. In *Proceedings of the 2006 IEEE Computer Society Conference on Computer Vision and Pattern Recognition (CVPR'06)*; IEEE: Piscataway, NJ, USA, 2006; Volume 2, pp. 2213–2220.
10. Song, J.; Xia, S.; Wang, J.; Chen, D. Curved buildings reconstruction from airborne LiDAR data by matching and deforming geometric primitives. *IEEE Trans. Geosci. Remote Sens.* **2020**, *59*, 1660–1674. [CrossRef]
11. Nan, L.; Wonka, P. Polyfit: Polygonal surface reconstruction from point clouds. In *Proceedings of the IEEE International Conference on Computer Vision*; IEEE: Piscataway, NJ, USA, 2017; pp. 2353–2361.
12. Li, M.; Wonka, P.; Nan, L. Manhattan-world urban reconstruction from point clouds. In *Proceedings of the European Conference on Computer Vision*; Springer: Berlin/Heidelberg, Germany, 2016; pp. 54–69.
13. Garland, M.; Heckbert, P.S. Surface simplification using quadric error metrics. In *Proceedings of the 24th Annual Conference on Computer Graphics and Interactive Techniques*; ACM: New York, NY, USA, 1997; pp. 209–216.
14. Li, M.; Nan, L. Feature-preserving 3D mesh simplification for urban buildings. *ISPRS J. Photogramm. Remote Sens.* **2021**, *173*, 135–150. [CrossRef]
15. Li, J.; Chen, D.; Hu, F.; Wang, Y.; Li, P.; Peethambaran, J. Shape-preserving mesh decimation for 3D building modeling. *Int. J. Appl. Earth Obs. Geoinf.* **2024**, *126*, 103623. [CrossRef]
16. Kazhdan, M.; Bolitho, M.; Hoppe, H. Poisson surface reconstruction. In *Proceedings of the Fourth Eurographics Symposium on Geometry Processing*; Eurographics Association: Goslar, Germany, 2006; Volume 7.
17. Bernardini, F.; Mittleman, J.; Rushmeier, H.; Silva, C.; Taubin, G. The ball-pivoting algorithm for surface reconstruction. *IEEE Trans. Vis. Comput. Graph.* **2002**, *5*, 349–359. [CrossRef]
18. Edelsbrunner, H.; Mücke, E.P. Three-dimensional alpha shapes. *ACM Trans. Graph. (Tog)* **1994**, *13*, 43–72. [CrossRef]

19. Kamra, V.; Kudeshia, P.; ArabiNaree, S.; Chen, D.; Akiyama, Y.; Peethambaran, J. Lightweight reconstruction of urban buildings: Data structures, algorithms, and future directions. *IEEE J. Sel. Top. Appl. Earth Obs. Remote Sens.* **2022**, *16*, 902–917. [CrossRef]
20. Glander, T.; Döllner, J. Abstract representations for interactive visualization of virtual 3D city models. *Comput. Environ. Urban Syst.* **2009**, *33*, 375–387. [CrossRef]
21. Xie, J.; Zhang, L.; Li, J.; Wang, H.; Yang, L. Automatic simplification and visualization of 3D urban building models. *Int. J. Appl. Earth Obs. Geoinf.* **2012**, *18*, 222–231. [CrossRef]
22. Dukai, B.; Ledoux, H.; Stoter, J. *3D Registration of Buildings and Addresses (BAG) Latest Data*; Urban Data Science: Delft, The Netherlands, 2019. [CrossRef]
23. Kada, M. Scale-dependent simplification of 3D building models based on cell decomposition and primitive instancing. In *Proceedings of the International Conference on Spatial Information Theory*; Springer: Berlin/Heidelberg, Germany, 2007; pp. 222–237.
24. Huang, H.; Brenner, C.; Sester, M. A generative statistical approach to automatic 3D building roof reconstruction from laser scanning data. *ISPRS J. Photogramm. Remote Sens.* **2013**, *79*, 29–43. [CrossRef]
25. Li, X.; Lin, Y.L.; Miller, J.; Cheon, A.; Dixon, W. Primitive-Based 3d building modeling, sensor simulation, and estimation. In *Proceedings of the IGARSS 2019—2019 IEEE International Geoscience and Remote Sensing Symposium*; IEEE: Piscataway, NJ, USA, 2019; pp. 5148–5151.
26. Schroeder, W.J.; Zarge, J.A.; Lorensen, W.E. Decimation of triangle meshes. In *Proceedings of the 19th Annual Conference on Computer Graphics and Interactive Techniques*; ACM: New York, NY, USA, 1992 ; pp. 65–70.
27. Soucy, M.; Laurendeau, D. Multiresolution surface modeling based on hierarchical triangulation. *Comput. Vis. Image Underst.* **1996**, *63*, 1–14. [CrossRef]
28. Rossignac, J.; Borrel, P. Multi-resolution 3D approximations for rendering complex scenes. In *Modeling in Computer Graphics: Methods and Applications*; Springer: Berlin/Heidelberg, Germany, 1993; pp. 455–465.
29. Luebke, D.; Erikson, C. View-dependent simplification of arbitrary polygonal environments. In *Proceedings of the 24th Annual Conference on Computer Graphics and Interactive Techniques*; ACM: New York, NY, USA, 1997; pp. 199–208.
30. Hoppe, H.; DeRose, T.; Duchamp, T.; McDonald, J.; Stuetzle, W. Mesh optimization. In *Proceedings of the 20th Annual Conference on Computer Graphics and Interactive Techniques*; ACM: New York, NY, USA, 1993; pp. 19–26.
31. Lindstrom, P.; Turk, G. Fast and memory efficient polygonal simplification. In *Proceedings of the Proceedings Visualization'98 (Cat. No. 98CB36276)*; IEEE: Piscataway, NJ, USA, 1998; pp. 279–286.
32. Haala, N.; Kada, M. An update on automatic 3D building reconstruction. *ISPRS J. Photogramm. Remote Sens.* **2010**, *65*, 570–580. [CrossRef]
33. CHEN, B.; SHE, J.; TAN, J.; MA, J.; WU, G. Research Progress on Simplification of Building Models in 3D Scenes. *Geomat. Inf. Sci. Wuhan Univ.* **2020**, *45*, 1429–1437.
34. Hoppe, H. New quadric metric for simplifying meshes with appearance attributes. In *Proceedings of the Proceedings Visualization'99 (Cat. No. 99CB37067)*; IEEE: Piscataway, NJ, USA, 1999; pp. 59–510.
35. Yao, L.; Huang, S.; Xu, H.; Li, P. Quadratic error metric mesh simplification algorithm based on discrete curvature. *Math. Probl. Eng.* **2015**, *2015*, 428917. [CrossRef]
36. LI, S.; HUO, L.; SHEN, T.; ZHU, J.; LI, P.; LIU, H. A simplification algorithm for edge collapse of 3D building model considering angle error. *Geomat. Inf. Sci. Wuhan Univ.* **2021**, *46*, 1209–1215.
37. Salinas, D.; Lafarge, F.; Alliez, P. Structure-aware mesh decimation. In *Proceedings of the Computer Graphics Forum*; Wiley Online Library: Hoboken, NJ, USA, 2015; Volume 34, pp. 211–227.
38. Xia, S.; Wang, R. A fast edge extraction method for mobile LiDAR point clouds. *IEEE Geosci. Remote Sens. Lett.* **2017**, *14*, 1288–1292. [CrossRef]
39. Biljecki, F.; Ledoux, H.; Du, X.; Stoter, J. The Most Common Geometric and Semantic Errors in CityGML Datasets. *Isprs Ann. Photogramm. Remote Sens. Spat. Inf. Sci.* **2016**, *IV-2/W1*, 13–22. [CrossRef]
40. buildingSMART International. Industry Foundation Classes, Version 4.0.2.1 (IFC4 ADD2 TC1). 2017. Available online: https://standards.buildingsmart.org/IFC/RELEASE/IFC4/ADD2_TC1/HTML/ (accessed on 2 December 2024).
41. Matrone, F.; Lingua, A.; Pierdicca, R.; Malinverni, E.S.; Paolanti, M.; Grilli, E. A Benchmark for Large-Scale Heritage Point Cloud Semantic Segmentation. *Int. Arch. Photogramm. Remote Sens. Spat. Inf. Sci.* **2020**, *XLIII-B2-2020*, 1419–1426. [CrossRef]
42. Wysocki, O.; Tan, Y.; Froech, T.; Xia, Y.; Wysocki, M.; Hoegner, L.; Cremers, D.; Holst, C. Zaha: Introducing the level of facade generalization and the large-scale point cloud facade semantic segmentation benchmark dataset. In *Proceedings of the 2025 IEEE/CVF Winter Conference on Applications of Computer Vision (WACV)*; IEEE: Piscataway, NJ, USA, 2025; pp. 7648–7658.
43. Zolanvari, S.; Ruano, S.; Rana, A.; Cummins, A.; Da Silva, R.E.; Rahbar, M.; Smolic, A. DublinCity: Annotated LiDAR point cloud and its applications. *arXiv* **2019**, arXiv:1909.03613.
44. Du, J.; Chen, D.; Zhang, Z.; Zhang, L. Research progress of building reconstruction via airborne point clouds. *Natl. Remote Sens. Bull.* **2021**, *23*, 374–391. [CrossRef]

45. Fan, H.; Meng, L.; Jahnke, M. Generalization of 3D buildings modelled by CityGML. In *Proceedings of the Advances in GIScience: Proceedings of the 12th AGILE Conference*; Springer: Berlin/Heidelberg, Germany, 2009; pp. 387–405.
46. Fan, H.; Meng, L. A three-step approach of simplifying 3D buildings modeled by CityGML. *Int. J. Geogr. Inf. Sci.* **2012**, *26*, 1091–1107. [CrossRef]
47. Zhu, J.; Wu, P.; Anumba, C. A semantics-based approach for simplifying IFC building models to facilitate the use of BIM models in GIS. *Remote Sens.* **2021**, *13*, 4727. [CrossRef]
48. Wu, J.; Shen, T.; Huo, L. Research on Lightweighting Methods for 3D Building Models Based on Semantic Constraints. *Int. Arch. Photogramm. Remote Sens. Spat. Inf. Sci.* **2025**, *48*, 1565–1571. [CrossRef]
49. Xia, W.; Luo, Y.; Fan, J.; Wang, S.; Liu, X.; Zhang, Y.; Fei, L.; Wang, W.; Zhang, B.; Zhang, J.; et al. Semantic-aware Multi-Scale Simplification of Urban-Scale 3D Real-Scene Mesh Models. *Int. Arch. Photogramm. Remote Sens. Spat. Inf. Sci.* **2025**, *48*, 333–340. [CrossRef]
50. Sketchfab, Inc. Sketchfab. Available online: https://sketchfab.com/ (accessed on 15 November 2025).
51. Gao, W.; Nan, L.; Boom, B.; Ledoux, H. SUM: A benchmark dataset of semantic urban meshes. *Isprs J. Photogramm. Remote Sens.* **2021**, *179*, 108–120. [CrossRef]
52. Chen, M.; Hu, Q.; Yu, Z.; Thomas, H.; Feng, A.; Hou, Y.; McCullough, K.; Ren, F.; Soibelman, L. STPLS3D: A Large-Scale Synthetic and Real Aerial Photogrammetry 3D Point Cloud Dataset. In Proceedings of the 33rd British Machine Vision Conference Proceedings, BMVC 2022, London, UK, 21–24 November 2022.
53. Sorkine, O.; Cohen-Or, D.; Lipman, Y.; Alexa, M.; Rössl, C.; Seidel, H.P. Laplacian surface editing. In *Proceedings of the 2004 Eurographics/ACM SIGGRAPH Symposium on Geometry Processing*; ACM: New York, NY, USA, 2004; pp. 175–184.
54. Sorkine, O.; Alexa, M. As-rigid-as-possible surface modeling. In Proceedings of the Symposium on Geometry Processing; ACM: New York, NY, USA, 2007; Volume 4, pp. 109–116.
55. Chen, Z.; Pan, Z.; Wu, K.; Vouga, E.; Gao, X. Robust low-poly meshing for general 3d models. *Acm Trans. Graph. (Tog)* **2023**, *42*, 1–20.
56. Oh, S.; Yuan, X.; Wei, X.; Shi, R.; Xiang, F.; Liu, M.; Su, H. PaMO: Parallel Mesh Optimization for Intersection-Free Low-Poly Modeling on the GPU. In *Proceedings of the Computer Graphics Forum*; Wiley Online Library: Hoboken, NJ, USA, 2025; Volume 44, p. e70267.